

Article

Economical-Environmental-Technical Operation of Power Networks with High Penetration of Renewable Energy Systems Using Multi-Objective Coronavirus Herd Immunity Algorithm

Ziad M. Ali ^{1,2,*} , Shady H. E. Abdel Aleem ³ , Ahmed I. Omar ⁴  and Bahaa Saad Mahmoud ⁴

- ¹ Electrical Engineering Department, College of Engineering, Prince Sattam bin Abdulaziz University, Wadi Addawaser 11991, Saudi Arabia
- ² Electrical Engineering Department, Aswan Faculty of Engineering, Aswan University, Aswan 81542, Egypt
- ³ Department of Electrical Engineering, Valley High Institute of Engineering and Technology, Science Valley Academy, Qalyubia 44971, Egypt; engyshady@ieee.org
- ⁴ Electrical Power and Machines Engineering Department, The Higher Institute of Engineering at El-Shorouk City, El-Shorouk Academy, Cairo 11837, Egypt; a.omar@sha.edu.eg (A.I.O.); b.saad@sha.edu.eg (B.S.M.)
- * Correspondence: dr.ziad.elhalwany@aswu.edu.eg

Abstract: This paper proposes an economical-environmental-technical dispatch (EETD) model for adjusted IEEE 30-bus and IEEE 57-bus systems, including thermal and high penetration of renewable energy sources (RESs). Total fuel costs, emissions level, power losses, voltage deviation, and voltage stability are the five objectives addressed in this work. A large set of equality and inequality constraints are included in the problem formulation. Metaheuristic optimization approaches—Coronavirus herd immunity optimizer (CHIO), salp swarm algorithm (SSA), and ant lion optimizer (ALO)—are used to identify the optimal cost of generation, emissions, voltage deviation, losses, and voltage stability solutions. Several scenarios are reviewed to validate the problem-solving competency of the defined optimisation model. Numerous scenarios are studied to verify the proficiency of the optimisation model in problem-solving. The multi-objective problem is converted into a normalized one-objective issue through a weighted sum-approach utilizing the analytical hierarchy process (AHP). Additionally, the technique for order preference by similarity to ideal solution (TOPSIS) is presented for identifying the optimal value of Pareto alternatives. Ultimately, the results achieved reveal that the proposed CHIO performs the other approaches in the EETD problem-solving.

Keywords: analytical hierarchy process (AHP); economical-environmental-technical dispatch; Coronavirus herd immunity optimizer (CHIO); renewable energy sources (RESs); TOPSIS

MSC: 39B12



Citation: Ali, Z.M.; Aleem, S.H.E.A.; Omar, A.I.; Mahmoud, B.S. Economical-Environmental-Technical Operation of Power Networks with High Penetration of Renewable Energy Systems Using Multi-Objective Coronavirus Herd Immunity Algorithm. *Mathematics* **2022**, *10*, 1201. <https://doi.org/10.3390/math10071201>

Academic Editors: Ioannis G. Tsoulos and Chuangyin Dang

Received: 20 January 2022

Accepted: 31 March 2022

Published: 6 April 2022

Publisher's Note: MDPI stays neutral with regard to jurisdictional claims in published maps and institutional affiliations.



Copyright: © 2022 by the authors. Licensee MDPI, Basel, Switzerland. This article is an open access article distributed under the terms and conditions of the Creative Commons Attribution (CC BY) license (<https://creativecommons.org/licenses/by/4.0/>).

1. Introduction

Using renewable energy sources (RESs) in conventional power grids is difficult since renewables have a stochastic nature. The expansion of the use of RES technologies has also shown that conventional thermal production plants face technoeconomic challenges. These challenges are of major significance if we are to overcome the complexities of renewable energy planning and facilitate seamless renewable integration of electricity grids that integrates the stochastic nature of photovoltaics, wind, and hydropower. To justify the investments in RES technologies, the grid must operate economically with a high level of dependability. In the sense of the climate [1], thermal stations emit many pollutants, including nitrogen oxides, carbon oxides, sulphur dioxides, and others [2]. Moreover, reduced network capacity losses, improved energy efficiency [3], voltage support, and investments will improve the power system operations. The formulation of the economical-environmental-technical dispatch (EETD) model will address this problem.

In the literature, the conventional economic, environmental, and technical dispatch problem was addressed by many traditional techniques, which were used to address optimization techniques, such as linear and quadratic iterative techniques [4], lambda iterating approaches [5], and gradient methods [6]. Since it is challenging to identify global solutions at a sufficient estimation period (computation time) because of the EETD problem's intricacy, most of these initiatives encountered challenges [7]. The researchers, therefore, sought to implement updated formulations of influential mathematical optimization approaches, such as mixed-integer linear (MIL) and quadratic (MIQ) programming type [8], nonlinear (NL) programming [9], and dynamics programming (DP) [10,11], to address the EETD issue. Many traditional mathematical optimization methods offered significant challenges when dealing with large-scale generation-incorporated power systems. They were frequently tipped into local minima because their preference coefficients appeared to vary through the optimization processes, which enhanced the estimation period considerably.

Recently, various metaheuristic optimization methods have been used in the literature, with and without the inclusion of the RESs for coping with the above-stated deficiencies of single objective (SO) and multi-objective (MO) functions [12,13]. Several evolutionary and metaheuristic optimisation methods have been used to effectively address the EETD problem, for instance: particle swarm optimization (PSO) through time-varying accelerating constant so-named TVAC-PSO [14]; accelerating PSO (APSO) [14]; modified MO moth-flame optimizer (MFO) [15]; modified whale optimization algorithm (MWOA) [16]; the internal search algorithm (ISA) [17]; criss-cross optimizer (CCO) [18]; a mixture of salp swarm optimizer (SSA) and PSO [19]; MO differential evolutionary based on summation (SMODE) [20]; enhanced SSA (ESSA) [21,22]; artificial bee colony (ABC) based on dynamic population, so-named ABC-DP [23], ABC [24]; MO population exterior optimizer (MOPEO) [25]; MO cross-entropy optimizer built on decomposition (MOCEO/D) [26]; and symbiotic organisms search (SOS) optimizer [27], as seen in Table 1.

Some have considered RESs, and some have not considered them while solving their problem of optimizations. Table 1 lists many recent research studies that have explored the role of RESs in the classical issue of EETD. Duman et al. [27] proposed the SOS technique to minimize cost functions, real power losses, voltage deviation, enhancement of contingency circumstances, and voltage stability. That approach was examined through IEEE 30-bus and IEEE 118-bus through incorporating RESs of wind, solar, and tidal energies. However, some constraints, such as prohibited operating zones (POZs) and valve point impacts, were not involved in the problem. Chen et al. [25] proposed the MOPEO technique for reducing costs and emissions for the IEEE 30-bus scheme and the inclusion of thermal, wind, and solar generating modules. The paper [28] proposed the NSGA-II with the reinforcement learning process, known as NSGA-RL, used to solve the MOEETD problems. The formulas for optimizing fuel costs and emissions were presented to include six thermal units incorporating the wind-power units. The results revealed that the NSGA-RL technique is successful in solving multi-objective EETD problems. However, it could be preferable to utilize more than one RES, such as solar or tidal power. The paper [20] introduced MOEA/D and SMODE techniques to minimize emission and cost functions in the IEEE 30-bus scheme, including the uncertainties of wind-, solar-, and tidal-power-producing units to address the MOEETD issue with a restricted number of thermal units. The paper [29] presented the thermal-, wind-, solar-, and tidal-power systems with a complex day-ahead stochastic scheduling, but only the cost of the fuel was involved in the optimization process. Elattar [30] proposed an enhanced shuffled-frog leaping-optimizer (ESFLO) to lessen fuel costs and emissions for MOEETD in combined power and heat units, with regard to the attendance of wind and solar power. Chinnadurrai and Victoire [18] presented a multi-objective CCO technique to minimize cost and emission functions with uncertain wind-energy units. That approach employed conventional multi-objective test functions and then ordinary complex EETD issues concerned with various wind-power integration ratios. The paper [31] proposed an enhanced sine cosine optimizer (ESCO) to solve different issues of EETD problems, such as costs, voltage profile, and power losses as a SO function.

Li et al. [32] presented the MOCHIO approach for solving dynamic EETD of hybrid RESs built on green certifications, although some limits increasing power flow were not explored in the problem. Table 1 lists some of the most recent studies on the presence and absence of RESs.

Table 1. Review of single and multi-objective EETD of thermal units in the presence and absence of RESs.

System	Ref.	IEEE System			Algorithms	Objective Functions					Decision-Making Tools	
		30-Bus	57-Bus	118-Bus		Economical	Environmental		Technical		AHP	TOPSIS
						Cost	Emission	P_{loss}	VD	$L-Index$		
IEEE without RESs	[26]	✓	-	✓	MOCE/D	✓	✓	-	-	-	-	-
	[31]	✓	-	✓	ESCA	✓	-	✓	✓	-	-	-
	[33]	✓	-	-	MOFA-CPA	✓	✓	-	-	-	-	-
	[34]	✓	-	-	MOMICA	✓	✓	✓	✓	-	-	-
	[35]	✓	✓	✓	I-NSGA-III	✓	✓	✓	✓	✓	-	-
	[36]	✓	-	-	ECHT	✓	-	-	✓	-	-	-
	[37]	✓	✓	-	DA-PSO	✓	✓	✓	-	-	-	-
	[38]	✓	-	-	SPEA	✓	-	✓	-	✓	-	-
	[39]	✓	-	✓	TLBO	✓	✓	✓	-	✓	-	-
	[40]	✓	✓	✓	KHA	✓	-	-	✓	✓	-	-
	[41]	-	✓	-	PSO	✓	✓	✓	✓	✓	-	-
	[42]	✓	✓	✓	MSA	✓	✓	✓	✓	✓	-	-
IEEE integrated with RESs	[13]	✓	-	-	MOHHO	✓	✓	-	-	-	-	-
	[20]	✓	-	-	MOEA/D & SMODE	✓	✓	-	-	-	-	-
	[25]	✓	-	-	MOPEO	✓	✓	-	-	-	-	-
	[28]	✓	-	-	NSGA-RL	✓	✓	-	-	-	✓	-
	[43]	✓	-	-	GSA	✓	✓	-	-	-	-	-
	[44]	✓	-	-	FFA & MGA	✓	✓	-	-	-	-	-
	[45]	✓	-	-	SMODE	✓	✓	-	-	-	-	-
	[46]	✓	-	-	MOEA/D	✓	✓	-	-	-	-	-
	[47]	✓	-	-	PBO	✓	-	-	-	-	-	-
	[48]	✓	-	-	NSGA-II	✓	✓	-	-	-	-	-
	[49]	✓	-	-	PSO	✓	✓	-	-	-	-	-
	[50]	✓	✓	-	EFPA & BFPA	✓	✓	-	-	-	-	-
[51]	✓	-	-	GABC	✓	✓	-	-	-	-	-	
[52]	✓	-	-	SSA & IGWO	✓	✓	✓	-	-	✓	-	
Proposed	✓	✓	-	CHIO & ALO & SSA	✓	✓	✓	✓	✓	✓	✓	

In this study, the IEEE 30-bus and IEEE 57-bus schemes are amended for integrating photovoltaic (PV), wind power (WP), and tidal power (TP) plants with a constrained number of thermal generations. The PV, WP, and TP uncertainties are discussed in-depth, utilizing suitable probability density functions (PDFs)—lognormal, Weibull, and Gumbel, respectively. The cost models presented in this study discuss the volatility and intermittent nature of the RESs, including underestimation of the penalty cost (UPC) and overestimation of the reservation cost (ORC). A Coronavirus herd immunity optimizer (CHIO), a salp swarm algorithm (SSA) [53], and an ant lion optimizer (ALO) [54] are employed as multi-objective and SO optimization approaches to identify the production cost as an economic benefit, emissions as an environmental benefit, losses (P_{loss}), voltage deviation (VD), and stability index ($L-index$) as a technical benefit. Various conditions are examined to demonstrate the suggested mode’s potential to meet this challenge. Moreover, a weighting sum policy utilizing the analytical hierarchy process (AHP) can be utilized for converting the MOEETD issue into a normalised SOEETD. In addition, as a single solution may be supported by the decision maker, the technique for order preference by similarity to the ideal solution (TOPSIS) classification tool was used to find a single alternative from the non-dominated solutions group of problems under survey. In the calculation process, the benefits of a TOPSIS measuring tool are consistency, simplicity, and understandability.

This article’s contributions are summarized as follows:

- Expression of the SOEETD and MOEETD problem considering thermal, PV, WP, and PVTP plants (integration of high penetration of various RESs) is investigated.
- Stochastic study of high penetration of RESs addressed has been accessible utilizing the appropriate PDFs.
- Various system restrictions including security, equality, inequality, and POZs constraints are investigated in the presented EETD problem.

- Various optimization approaches, such as the CHIO, the ALO, and the SSA, with a comprehensive study of the solutions are used to solve the EETD problem.
- The AHP is utilized to convert MOEETD into the SOEETD problem.
- The TOPSIS is applied for obtaining the optimum alternative for the MOEETD issue.

The rest of the paper is structured as follows: The formation of the systems of SOEETD and MOEETD is demonstrated in Section 2. Section 3 describes the mathematical model of the high penetration of RESs, the formulation of SO and MO objectives, and the conception of limitations. Section 4 presents the recommended optimization strategies. The results are examined and discussed in Section 5. Lastly, Section 6 presents conclusions and future works.

2. Systems Investigated and Scenarios Studies

The first phase of this study is the development of ideal location buses for RESs. The design criteria to find the best location of RESs is corresponding to the optimum EETD issue when the PV, WP, and PVTP are inserted on all buses one by one. The optimal power flow (OPF) is used to add PV panels one by one, starting with bus two and working through all the buses in each system. The bus with the lowest cost for 24 h is the best candidate for PV panels. The OPF is also used to optimize the site of WP and PVTP using the same method as the PV panel optimal sitting as long as the PV panels are installed on the previously selected buses. The capacities of these plants are selected to be consistent with the test systems' maximum demands. The simulation results of this phase, which are the ideal location for the RESs for each of IEEE 30-bus and IEEE 57-bus testing schemes, are presented in Table 2. These locations of RESs are employed in the EETD problem, and the next step of this study is the uncertainties of RESs and are given in detail in the next section.

Table 2. Optimal location of the RESs in the IEEE 30-bus and IEEE 57-bus schemes.

Systems	IEEE30-Bus	IEEE57-Bus
Photovoltaic (PV)	Bus 11	Bus 3
Wind (WP)	Bus 5	Bus 2
PV + Tidal power (PVTP)	Bus 13	Bus 9

This work integrates both traditional thermal stations and non-conventional RESs that address the IEEE 30-bus and IEEE 57-bus schemes. As depicted in Figure 1, various significant RESs of PVs, wind, and hybrid PVs and tidal power (PVTP) schemes for the IEEE 30-bus are tied on buses 11, 5, and 13, respectively. In addition, the RESs of PVs wind and PVTP for the IEEE 57-bus are tied on buses 3, 2, and 9, respectively. The IEEE 30-bus system also includes three thermal power generations (TPGs) tied on buses 1, 2, and 8. In addition, the IEEE 57-bus scheme includes four TPGs tied on buses 1, 6, 8, and 12. The necessary system's specifications are described in Table 3.

Table 3. Parameters of the IEEE30-bus and IEEE57-bus systems [55].

Elements	IEEE30-Bus		IEEE57-Bus	
	Quantity	Parameters	Quantity	Parameters
Generators	6	3 TPGs and 3 RESs	7	4 TPGs and 3 RESs
TPGs	3	Buses 1(swing), 2, and 8	4	Buses 1 (swing), 6, 8, and 12
RESs	PV	Bus 11, 75 MW	75	Bus 3, 175 MW
	WP	Bus 5, 50 MW	1	Bus 2, 90 MW
	PVTP	Bus 13, 45 + 5 MW	1	Bus 9, 75 + 15 MW
Static VAR compensator	9	Buses 10, 12, 15, 17, 20, 21, 23, 24, and 29	3	Buses 18, 25, and 53
Load connected (<i>P</i> and <i>Q</i>)	-	283.40 MW and 126.20 MVar	-	1250.80 MW and 336.40 MVar
Number of PQ buses	24	24 buses	50	50 buses
Load voltage permissible range (pu)	-	0.950–1.10	-	0.950–1.10

of objectives. The first scheme will present 13 case studies: the IEEE 30-bus system. In scenarios 14 to 16, the second scheme of the IEEE 57-bus will be introduced. These scenarios represent one and MOs that indicate different economic, environmental, and technical issues.

Table 4. Description of SOEETD and MOEETD formulation.

Test System	EETD Formulation		Economical	Environmental	Technical			
	No. of Objective Functions	Scenario	Fuel Costs	Emissions	VD	P_{loss}	$L-Max$	
IEEE-30	1	1	✓					
		2		✓				
		3				✓		
		4					✓	
		5						✓
	2	6	✓	✓		✓		
		7	✓			✓		
		8	✓			✓	✓	
		9	✓			✓	✓	✓
		10	✓			✓	✓	
	3	11	✓	✓	✓	✓		
		12	✓	✓	✓	✓	✓	
		13	✓	✓	✓	✓	✓	✓
IEEE-57	1	14	✓					
	2	15	✓		✓			
		16	✓	✓				

3. Formulation of the Optimization Problems

The EETD issue is implemented by simultaneously minimizing numerous computing objectives—fuel costs, emissions, voltage deviation, power losses, and enhancement of line index (*L-index*)—taking into account various constraints. In general, the EETD issue can be outlined as the following:

$$J_{obj} = \min \sum_{i=1}^{N_{obj}} J_i(x, v) \tag{1}$$

Subject to

$$g_k(x, v) = 0 \quad k = 0, 1, \dots, G \tag{2}$$

$$h_l(x, v) \leq 0 \quad l = 0, 1, \dots, L \tag{3}$$

where J_{obj} represents the objectives to be minimized. $J_1, J_2, J_3, J_4,$ and J_5 represent the quanta-objectives to be minimized. They represent the fuel costs, emissions, voltage deviation, losses, and *L-index*, respectively. x signifies the state (dependent) variables, and v represents the control variables. $g_k(x, v)$ and $h_l(x, v)$ represent the k^{th} equality constraints and the l^{th} inequality constraints, respectively.

3.1. Total Fuel Costs

The total costs of the produced powers are the sum of costs of the TPGs and RESs, as expressed in Equation (4).

$$J_1(x, v) = C_{tot}(P_{TPGs}) + C_{tot}(P_{RESs}) \tag{4}$$

where $C_{tot}(P_{TPGs})$ denotes the total TPGs cost, and $C_{tot}(P_{RESs})$ denotes the total RESs cost.

3.1.1. Fuel-Cost Study of TPG Units

The costs of TPGs in \$/MWh depend more on the blades' steam flow of the turbine and the unpredicted fluctuations in a valve's position. In such plants, a series of valves push steam through a scattered set of nozzles that are used to deliver good output in full

production [39]. The valves are sequentially opened for compulsory output, resulting in the interruption costs curve, as seen in Figure 2. Equation (5) provides the cost formulation of TPGs [30].

$$C_{tot}(P_{TPGs}) = \sum_{i=1}^{N_{TPG}} a_{TPG_i} + b_{TPG_i} P_{TPG_i} + c_{TPG_i} P_{TPG_i}^2 + \left| d_i \sin \left(e_i \left(P_{TPG_i}^{min} - P_{TPG_i} \right) \right) \right| \quad (5)$$

where N_{TPG} denotes the number of thermal generator units. a_{TPG_i} , b_{TPG_i} , and c_{TPG_i} denote the cost coefficients of the i th thermal generator unit (P_{TPG_i}). The two coefficients d_i and e_i denote the impact's valve point. $P_{TPG_i}^{min}$ denotes the minimum powers of P_{TPG_i} through the generator operations. These parameters are described in Table 5.

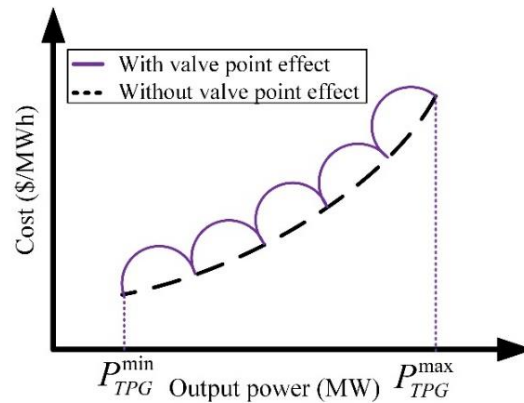


Figure 2. The cost of fuel functions with and without the effect of valve point.

Table 5. Emission and cost coefficients for IEEE 30-bus and IEEE 57-bus of the TPGs [30].

Emission coefficients						
Generators	Bus	φ_{TPG} (t/h)	ψ_{TPG} (t/pu·MWh)	ω_{TPG} (t/pu·MW ² h)	τ_{TPG} (t/h)	ζ_{TPG} (pu·MW ⁻¹)
IEEE 30-bus						
TPG ₁	1	0.04092	−0.05553	0.0649	0.0003	6.668
TPG ₂	2	0.02543	−0.06048	0.05639	0.0006	3.334
TPG ₃	8	0.05327	−0.0356	0.0339	0.003	2
IEEE 57-bus						
TPG ₁	1	4.091	−5.554	6.49	0.0002	0.286
TPG ₂	6	2.543	−6.047	5.638	0.0005	0.333
TPG ₃	8	6.131	−5.55	5.151	0.0001	0.667
TPG ₄	12	3.491	−5.754	6.39	0.0003	0.266
Cost coefficients						
Generators	Bus	a_{TPG} (\$/h)	b_{TPG} (\$/MWh)	c_{TPG} (\$/MW ² h)	d_{TPG} (\$/h)	e_{TPG} (MW ⁻¹)
IEEE 30-bus						
TPG ₁	1	30	2	0.00377	18	0.038
TPG ₂	2	25	1.76	0.0176	16	0.039
TPG ₃	8	20	3.26	0.00833	12	0.046
IEEE 57-bus						
TPG ₁	1	0	20	0.0775795	18	0.037
TPG ₂	6	0	40	0.01	16	0.038
TPG ₃	8	0	20	0.02222	13.5	0.041
TPG ₄	12	0	20	0.03226	18	0.037

3.1.2. Fuel-Cost Study of the RESs

The cost's RESs are the sum of the overall costs of WPs ($C_{tot}(P_{WP})$), PVs ($C_{tot}(P_{PV})$), and hybrid PV and PVTP ($C_{tot}(P_{PVTP})$), which can be expressed as shown in Equation (6):

$$C_{tot}(P_{RESs}) = C_{tot}(P_{WP}) + C_{tot}(P_{PV}) + C_{tot}(P_{PVTP}) \tag{6}$$

However, there is a cost feature for each renewable source. The sum of energy that is undersupplied or oversupplied may also be estimated relying on the PDFs of each source. First, standby power-generating (SPG) units may be mounted to meet the intermittent nature of the RESs while the produced power is lower than the power scheduled. Second, energy storage (ES) could be mounted to store the additional power produced [56].

In accordance with random wind speed, solar irradiance, and tidal unit flow rate results, Weibull, lognormal, and Gumbel distributions are used to convey the cost terms as seen as follows.

Cost estimation of WPs ($C_{tot}(P_{WP})$) : $C_{tot}(P_{WP})$ is described by merging the investment costs ($C_{d_{WP}}(P_{WPsch})$) directly besides storage units' costs and the SPGs. $C_{d_{WP}}(P_{WPsch})$ denotes the costs of operation and maintenance as follows:

$$C_{d_{WP}}(P_{WPsch}) = K_{d_{WP}}P_{WPsch} \tag{7}$$

where $K_{d_{WP}}$ signifies the direct cost coefficient, and P_{WPsch} signifies the WPs' power scheduled. The scheme also could involve possible standby elements to conserve the demand desires, and this reserve cost capacity ($C_{r_{WP}}$) can be expressed as follows:

$$C_{r_{WP}}(P_{WPsch} - P_{WPact}) = K_{r_{WP}}(P_{WPsch} - P_{WPact}) = K_{r_{WP}} \int_0^{P_{WPact}} (P_{WPsch} - p_{WP})f_{WP}(p_{WP})dp_{WP} \tag{8}$$

$K_{r_{WP}}$ signifies the cost coefficient of the standby elements, and P_{WPact} signifies the real WPs' power delivered. $f_{WP}(p_{WP})$ denotes the wind PDF. p_{WP} represents the WGs' supplied power. Similarly, if $P_{WPsch} < P_{WPact}$; also, the ES' cost ($C_{s_{WP}}$), described in (9), should be appended to the WP cost. The cost factors of WPs can be expressed in Appendix A.

$$C_{s_{WP}}(P_{WPact} - P_{WPsch}) = K_{s_{WP}}(P_{WPact} - P_{WPsch}) = K_{s_{WP}} \int_{P_{WPsch}}^{P_{WPpr}} (p_{WP} - P_{WPsch})f_{WP}(p_{WP})dp_{WP} \tag{9}$$

where $K_{s_{WP}}$ and P_{WPpr} denote the penalty cost factor and the rated wind power, respectively. The standby powers and storage units can be dependent on $f_{WP}(p_{WP})$. Weibull fitting (WF) is commonly used to fit the random frequency of each v measure [57,58]. Figure 3a shows the WF-based PDF of v data spreading over 8000 Monte-Carlo runs. The scale (α) and the shape (β) coefficients of the WF-based PDF are considered as nine and two, respectively. The probability ($f_v(v)$) of v is shown in (10):

$$f_v(v) = \left(\frac{\beta}{\alpha}\right) \left(\frac{v}{\alpha}\right)^{(\beta-1)} e^{-\left(\frac{v}{\alpha}\right)^\beta} \text{ for } 0 < v < \infty \tag{10}$$

The WGs' supplied power that be dependent on v is expressed as follows:

$$p_{WP} = \begin{cases} 0 & v_{out} \leq v \leq v_{in} \\ P_{WPpr} \left(\frac{v-v_{in}}{v_r-v_{in}}\right) & v_{in} \leq v \leq v_r \\ P_{WPpr} & v_r \leq v \leq v_{out} \end{cases} \tag{11}$$

where v_{in} , v_{out} , v_r correspond to the WPs' cut-in, cut-out, and rated speeds, respectively. The probability's WP ($f_{WP}(p_{WP})$) is given in (12).

$$f_{WP}(p_{WP}) = \frac{\beta(v_r - v_{in})}{\alpha^\beta P_{WPpr}} \left[v_{in} + \frac{p_{WP}}{P_{WPpr}}(v_r - v_{in}) \right]^{\beta-1} \exp \left[- \left(\frac{v_{in} + \frac{p_{WP}}{P_{WPpr}}(v_r - v_{in})}{\alpha} \right)^\beta \right] \tag{12}$$

To sum up, $C_{tot}(P_{WP})$ is expressed in (13).

$$C_{tot}(P_{WP}) = C_{d_{WP}}(P_{WP_{sch}}) + C_{r_{WP}}(P_{WP_{sch}} - P_{WP_{act}}) + C_{s_{WP}}(P_{WP_{act}} - P_{WP_{sch}}) \quad (13)$$

Cost estimation of the PV ($C_{tot}(P_{PV})$): As well, the WPs' cost function, the direct cost $C_{d_{PV}}(P_{PV_{sch}})$ of PVs signifies the costs of operation and maintenance and can be described as follows:

$$C_{d_{PV}}(P_{PV_{sch}}) = K_{d_{PV}}P_{PV_{sch}} \quad (14)$$

where $K_{d_{PV}}$ denotes the direct cost parameter, and $P_{PV_{sch}}$ signifies the scheduled power of PV.

Once $P_{PV_{sch}}$ is superior to the PV system's real power ($P_{PV_{act}}$), it is crucial to calculate SPGs, as clarified previously. The PV's cost reserve capacity ($C_{r_{PV}}$) can be expressed as follows:

$$C_{r_{PV}}(P_{PV_{sch}} - P_{PV_{act}}) = K_{r_{PV}}(P_{PV_{sch}} - P_{PV_{act}}) = K_{r_{PV}}(P_{PV_{sch}} - p_{PV})f_{PV}(p_{PV}) \quad (15)$$

$K_{r_{PV}}$ signifies the cost coefficient of the SPGs. $f_{PV}(p_{PV})$ denotes the PV-PDF. p_{PV} represents the PVs' supplied power. Moreover, the cost of storage units ($C_{s_{PV}}$) may appear if $P_{PV_{sch}} < P_{PV_{act}}$, and this is expressed in (16).

$$C_{s_{PV}}(P_{PV_{act}} - P_{PV_{sch}}) = K_{s_{PV}}(P_{PV_{act}} - P_{PV_{sch}}) = K_{s_{PV}}(p_{PV} - P_{PV_{sch}})f_{PV}(p_{PV}) \quad (16)$$

The cost parameters of PV can be additionally offered in Appendix A. The power provided from the backup and ES units depends on the solar irradiance (G) PDF, represented as $f_{PV}(G)$. Lognormal fitting (LF) [59,60] can be frequently utilized to obtain $f_{PV}(G)$, as depicted in Figure 3b for 8000 Monte-Carlo turns at lognormal fit parameters: $\mu = 5.6$ and $\sigma = 0.6$. Consequently, $f_{PV}(G)$ is expressed as follows:

$$f_{PV}(G) = \frac{1}{G\sigma\sqrt{2\pi}} \exp\left\{-\frac{(\ln G - \mu)^2}{2\sigma^2}\right\}, \quad \forall G > 0 \quad (17)$$

The attainable PV's power ($p_{PV}(G)$) can be assessed as follows

$$p_{PV}(G) = \begin{cases} P_{PVr}\left(\frac{G^2}{G_{std}}\right), & 0 < G < R_c \\ P_{PVr}\left(\frac{G}{G_{std}}\right), & G \geq R_c \end{cases} \quad (18)$$

where G_{std} signifies the traditional solar irradiance, and R_c signifies the operation irradiance, wherein $G_{std} = 1000 \text{ W/m}^2$, and $R_c = 120 \text{ W/m}^2$. P_{PVr} signifies the PVs rated power output. To summarize, $C_{tot_{PV}}$ can be described as follows:

$$C_{tot}(P_{PV}) = C_{d_{PV}}(P_{PV_{sch}}) + C_{s_{PV}}(P_{PV_{act}} - P_{PV_{sch}}) + C_{r_{PV}}(P_{PV_{sch}} - P_{PV_{act}}) \quad (19)$$

Cost estimation of the PVTP plant ($C_{tot}(P_{PVTP})$): Gumbel fitting (GF) [61] is employed in the river flow's fitting of (Q_w) statistics, as displayed in Figure 3c, wherein $f_Q(Q_w)$ traces the GD through coefficients λ and γ as the following:

$$f_Q(Q_w) = \frac{1}{\gamma} \exp\left(\frac{Q_w - \lambda}{\gamma}\right) \exp\left[-\exp\left(\frac{Q_w - \lambda}{\gamma}\right)\right] \quad (20)$$

The yield power from the tidal power plant $P_T(Q_w)$ relies on Q_w as expressed in (19):

$$P_T(Q_w) = \eta_w \rho_w g_w Q_w H_w \quad (21)$$

where η_w , g_w , ρ_w , and H_w signify the tidal efficiency turbines', the gravity acceleration, the density's water, and the operational head pressure, respectively [62], wherein $\eta_w = 0.86$;

$\rho_w = 1000 \text{ kg/m}^3$; $g_w = 9.81 \text{ m/s}^2$; and $H_w = 26 \text{ m}$. At this bus, the TP unit is incorporated through a PV unit to enhance the TP station operation. To summarize, $C_{totPVTP}$ can be illustrated as follows:

$$C_{tot}(P_{PVTP}) = C_{dPVTP}(P_{PVTPsch}) + C_{rPVTP}(P_{PVTPsch} - P_{PVTPact}) + C_{sPVTP}(P_{PVTPact} - P_{PVTPsch}) \quad (22)$$

where $P_{PVTPsch}$ and $P_{PVTPact}$ signify the hybrid PVTP’s scheduled and real powers, respectively. $C_{dPVTP}(P_{PVTP})$ signifies the PVTP direct cost. The PVTP’s cost reserve capacity can be denoted as (C_{rPVTP}). The storage units cost of the PVTP system can be denoted as (C_{sPVTP}). The cost parameters of PVTP can be described in Appendix A.

Furthermore, the whole cost of the arrangement can be described as follows:

$$J_1(x, v) = \sum_{i=1}^{N_{TPG}} a_{TPG_i} + b_{TPG_i} P_{TPG_i} + c_{TPG_i} P_{TPG_i}^2 + \left| d_i \sin \left(e_i \left(P_{TPG_i}^{min} - P_{TPG_i} \right) \right) \right| + C_{dWP}(P_{WPsch}) + C_{rWP}(P_{WPsch} - P_{WPact}) + C_{sWP}(P_{WPact} - P_{WPsch}) + C_{dPV}(P_{PVsch}) + C_{rPV}(P_{PVsch} - P_{PVact}) + C_{sPV}(P_{PVact} - P_{PVsch}) + C_{dPVTP}(P_{PVTPsch}) + C_{rPVTP}(P_{PVTPsch} - P_{PVTPact}) + C_{sPVTP}(P_{PVTPact} - P_{PVTPsch}) \quad (23)$$

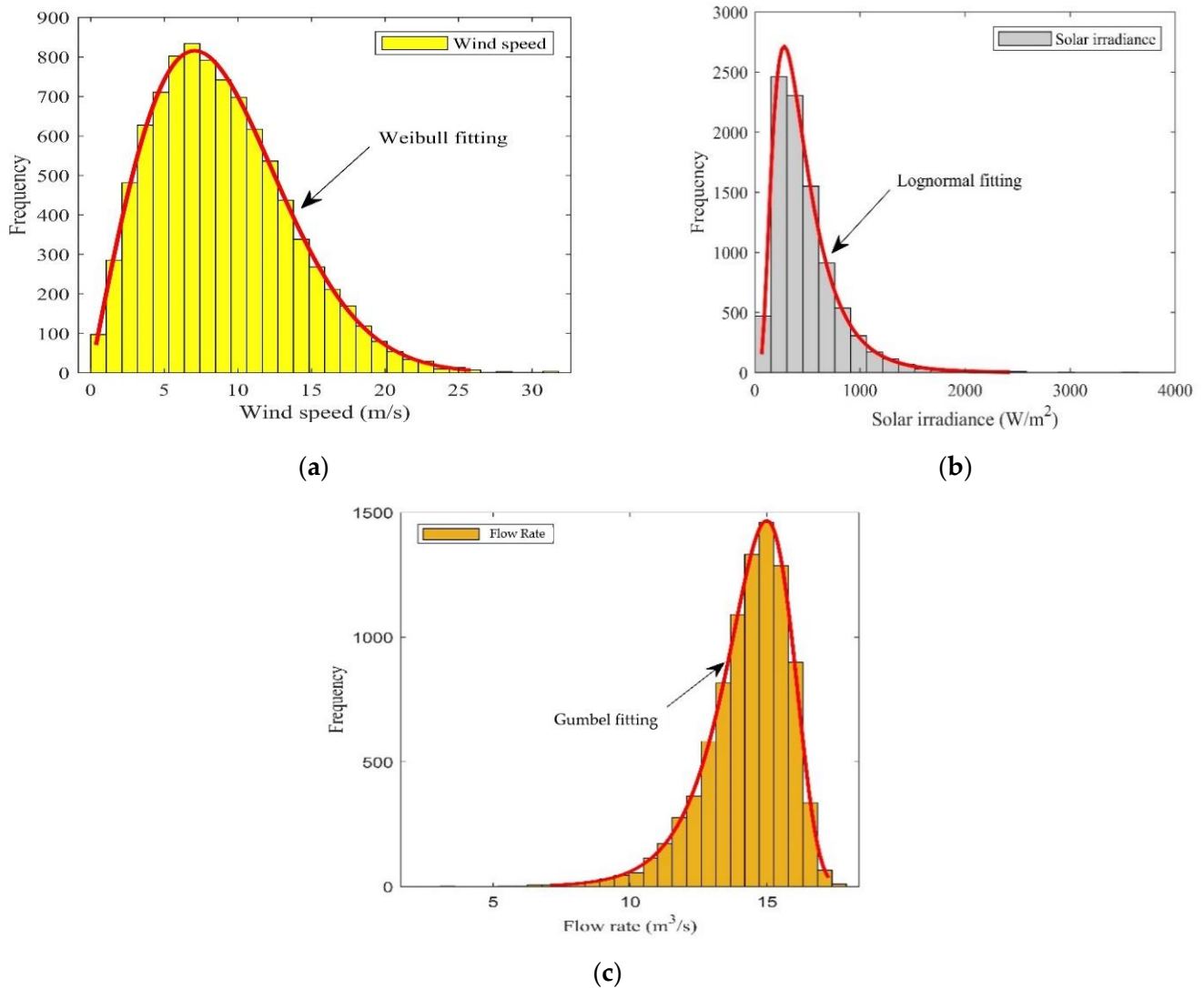


Figure 3. Measured PDFs of WP, PV irradiance, and tidal: (a) WF; (b) LF; and (c) GF.

3.2. Emission Levels

Only the emission levels of TPGs (E_{tot}) are addressed because the RESs have few to no pollutant gases, as given in (24):

$$J_2(x, v) = E_{tot} = \sum_{i=1}^{N_{TPG}} [\varphi_{TPG_i} + \psi_{TPG_i} P_{TPG_i} + \omega_{TPG_i} P_{TPG_i}^2 + \tau_{TPG_i} e^{\xi_{TPG_i} P_{TPG_i}}] \quad (24)$$

where E_{tot} signifies the overall emissions of the i th TPG. φ_{TPG_i} , ψ_{TPG_i} , ω_{TPG_i} , τ_{TPG_i} , and ξ_{TPG_i} are the coefficients of pollutant emissions related to the i th TPGs and are tabulated in Table 5.

3.3. Voltage Deviation

The fourth goal is to minimize the voltage deviations (ΔV) that could be described as follows:

$$J_3(x, v) = \Delta V = \sum_{i=1}^{N_{bus}} |V_i - 1| \quad (25)$$

where V_i and N_{bus} indicate i th bus voltages and the number of buses, respectively.

3.4. Power Losses

The third goal is to lessen the real losses (P_{loss}) of the electric utility that can be described as follows:

$$J_4(x, v) = P_{loss} = \sum_{i=1}^{N_G} [V_i^2 + V_j^2 - 2V_i V_j \cos(\delta_{ij})] \quad (26)$$

where N_G denotes the number of generator buses. V_i and V_j correspond to i and j bus voltages, respectively. $\delta_{ij} = \delta_i - \delta_j$ signifies the voltage phase shift variation between i and j buses.

3.5. Voltage Stability Metric

To improve system's voltage stability, it intends to lessen the maximum voltage stability index (L -index) that is described by Equations (27) and (28):

$$J_5(x, v) = L - index = \left| 1 - \sum_{i=1}^{N_G} F_{ij} \frac{V_i}{V_j} \angle(\theta_{ij} + \delta_i - \delta_j) \right| \quad (27)$$

$$F_{ij} = -|Y_{LL}|^{-1} |Y_{LG}| \quad (28)$$

3.6. Constraints

The limitations judged while implementing the OP can be summarized as the following.

3.6.1. Power Balance

The restrictions to stabilize the real and reactive powers through the total load powers consumed and the losses of the power can be expressed as the following:

$$P_{TPG} = P_{L_i} + P_{Loss_i} \quad (29)$$

$$Q_{TPG} = Q_{L_i} + Q_{Loss_i} \quad (30)$$

3.6.2. Limits of the Active and Reactive Powers

The operation limits for active and reactive powers of the TPGs, WPs, PVs, and PVTP are expressed as follows:

$$P_{TPG_i}^{min} \leq P_{TPG_i} \leq P_{TPG_i}^{max} \quad \forall i \in N_{TPG} \quad (31)$$

$$P_{WP}^{min} \leq P_{WP} \leq P_{WP}^{max} \tag{32}$$

$$P_{PV}^{min} \leq P_{PV} \leq P_{PV}^{max} \tag{33}$$

$$P_{PVTP}^{min} \leq P_{PVTP} \leq P_{PVTP}^{max} \tag{34}$$

$$Q_{TPG_i}^{min} \leq Q_{TPG_i} \leq Q_{TPG_i}^{max} \quad \forall i \in N_{TPG} \tag{35}$$

$$Q_{WP}^{min} \leq Q_{WP} \leq Q_{WP}^{max} \tag{36}$$

$$Q_{PV}^{min} \leq Q_{PV} \leq Q_{PV}^{max} \tag{37}$$

$$Q_{PVTP}^{min} \leq Q_{PVTP} \leq Q_{PVTP}^{max} \tag{38}$$

3.6.3. Limits of POZs

POZs, the aim for cutting off in the process of the TPGs, can be described in (39):

$$P_{TPG_i}^{minPOZ,j} \leq POZ_{TPG_i}^j \leq P_{TPG_i}^{maxPOZ,j} \tag{39}$$

where $P_{TPG_i}^{minPOZ,j}$ and $P_{TPG_i}^{maxPOZ,j}$ signify the minimum and maximum boundaries (MW) of the j th POZ of the i th TPG.

3.6.4. Security Restrictions

The generators and voltage at load buses' boundaries can be described in (40) and (41), respectively. In addition, the thermal limits can be considered as follows:

$$V_{G_i}^{min} \leq V_{G_i} \leq V_{G_i}^{max} \quad \forall i \in N_G \tag{40}$$

$$V_{L_j}^{min} \leq V_{L_j} \leq V_{L_j}^{max} \quad \forall j \in N_L \tag{41}$$

$$S_{L_j} \leq S_{L_j}^{max} \quad \forall j \in nl \tag{42}$$

where V_{G_i} , V_{L_j} denote the i th's generator bus voltage and the j th's load bus voltage, respectively. N_G , N_L , and nl indicate the generator buses, load buses, and branches numbers, respectively.

Multi-objective problems may be subjected to linear, nonlinear, equality, and inequality constraints. The inequality constraints of other variables are included in the objective functions using a death penalty factor (P) by adding an extremely high value to the objective functions to avoid infeasible solutions (when a solution violates a constraint, it will be rejected). P is set to 10^8 in the optimization problem investigated.

4. Coronavirus Herd Immunity Optimizer (CHIO)

Mathematically, the notion of herd protection can be modeled to build the fundamental CHIO technique [63]. The methodological approach depends on the notion that humanity protects against infection by changing the majority of the non-infected vulnerable to immune [64]. Consequently, the protected population will no longer propagate this virus; even those vulnerable instances would not be harmed. The populations of people with herd protection could be categorized into resistant, susceptible, and infectious. The CHIO formulation is built on the population of the herd protection as shown in Figure 4. The improvement technique is derived from susceptible, contaminated, and immunized persons in the execution method of the CHIO technique. With the CHIO algorithm, the definition of societal distance is achieved by splitting the individual from the community that may be vulnerable, diseased, or protected between the present individual and a particular individual. The method to herd protection is based on the CHIO methodology. The algorithm is developed in six main phases. The technique for implementation is as follows.

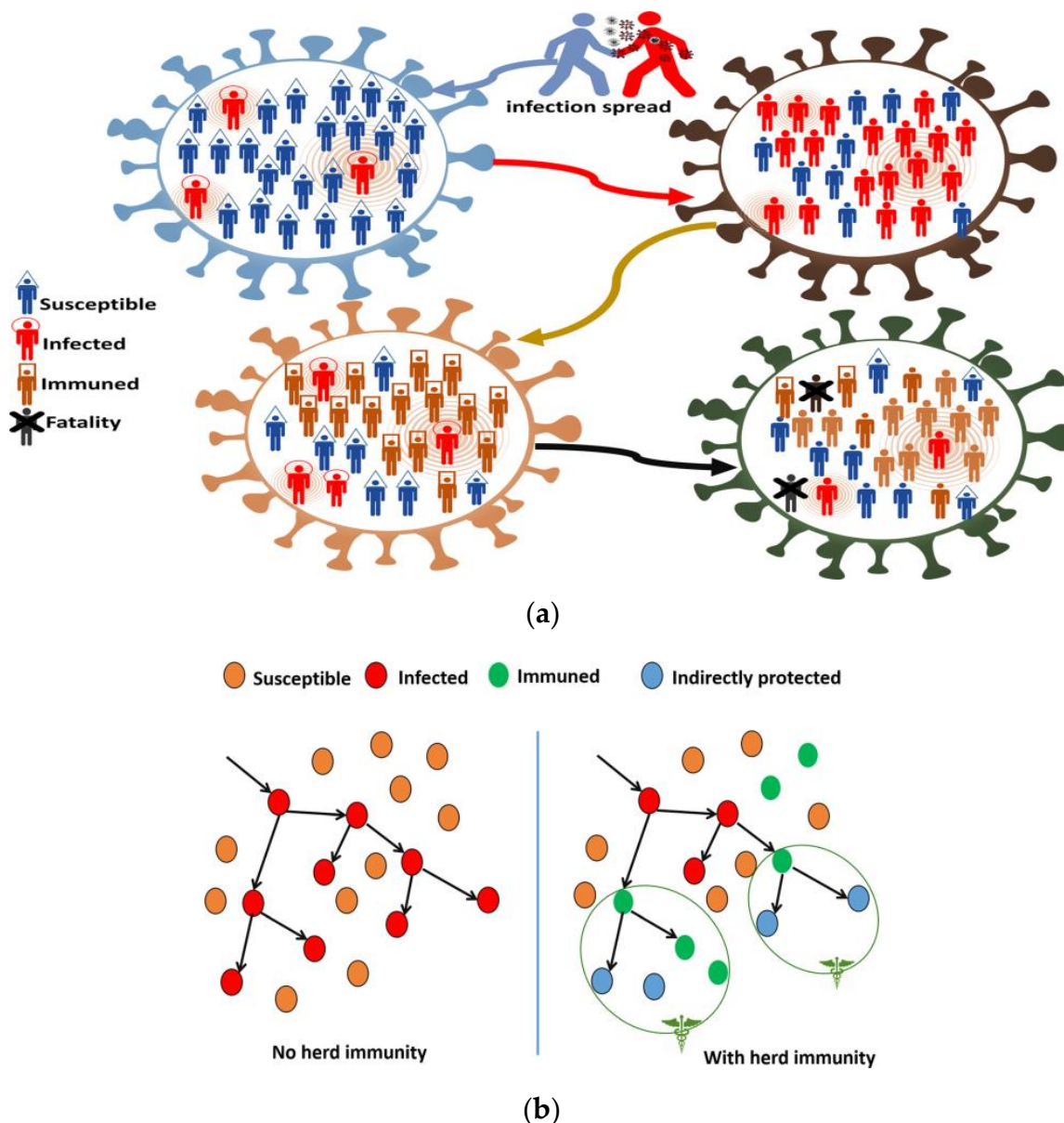


Figure 4. Herd immunity: (a) population; and (b) hierarchy [63].

Rule #1: Set CHIO parameter—The CHIO objective function is:

$$\min_x f(x), \quad x \in [lb, ub] \tag{43}$$

where for all the individuals, the objective function is created, in which the variable of decision is x_i , and indexed with “i”, and the gene number in everyone is indicated as n . The CHIO approach needs dual control factors, such as maximum diseased cases age (Max_{Age}) and fundamental reproduction rate (BR_r), and four algorithmic factors, such as $C_0 (=1)$, Max_Itr represents maximum iteration number, HIS represents the size of herd immunity, and n indicates size.

Rule #2: Generate herd immunity populations (HIP)—Originally, the CHIO generates heuristically a number of persons such as *HIS*. As a bidimensional matrix, the created individuals are kept in the *HIP* as follows:

$$HIP = \begin{bmatrix} x_1^1 & \dots & x_n^1 \\ \vdots & \ddots & \vdots \\ x_1^{HIS} & \dots & x_n^{HIS} \end{bmatrix} \tag{44}$$

For each person, the best solution is derived using Equation (44). The status trajectory (*S*) is also determined by either zero or one for all individuals in the *HIP*. Please note that *S* numbers are randomly begun up to C_0 .

Rule #3: Herd immunity evolution—It is the principal upgrade loop of CHIO. The individual gene gives the same or publicly differentiated influence, according to the BR_r , by using three principles:

$$x_i^j(t+1) = \begin{cases} x_i^j(t), & r \geq BR_r \\ C(x_i^j(t)), & r < 0.333 \times BR_r \text{ (Infected)} \\ N(x_i^j(t)), & r < 0.667 \times BR_r \text{ (Susceptible)} \\ R(x_i^j(t)), & r < BR_r \text{ (Immuned)} \end{cases} \tag{45}$$

where r signifies an arbitrary number from $[0, 1]$. The diseased situation is in the range of 0 to $0.333 \times BR_r$. The importance of the latest gene can be diminished by societal distance and can be obtained by the differences among the genes from the diseased situation and the present gene as the following.

$$x_i^j(t+1) = C(x_i^j(t)) \tag{46}$$

$$C(x_i^j(t)) = x_i^j(t) + r \times (x_i^j(t) - x_i^c(t)) \tag{47}$$

Similarly, the susceptible case can be in the range of $0.333 \times BR_r$ to $0.667 \times BR_r$. In addition, the safe case is in the range of $0.667 \times BR_r$ to BR_r .

Rule #4: Population update—The protection rate can be computed for each produced instance, but the existing alternative will only be replaced through the produced issue if $f(x^j(t+1)) < f(x^j(t))$. If the status vector S_j is equally one, the age vector (A_j) is incremented to one. The values of S_j are changed by the following equation throughout each cycle, according to the herd immunologic threshold.

$$S_j = \begin{cases} 1, & f(x^j(t+1)) < \frac{f(x^j(t+1))}{\Delta f(x)} \wedge S_j = 0 \wedge is_Corona(x^j(t+1)) \\ 2, & f(x^j(t+1)) < \frac{f(x^j(t+1))}{\Delta f(x)} \wedge S_j = 1 \end{cases} \tag{48}$$

where $is_Corona(x^j(t+1))$ is equally one, that is a binary quantity when a new situation has taken advantage of infected cases.

Rule #5: Casualty cases—If the protection rate of the present afflicted case might not arise for the required iteration, as provided in the Max_{Age} parameter, then this process is deemed dead. It is then regenerated from the scratched utilizing $x_i^j(t+1) = lb_i + (ub_i - lb_i) \times U(0, 1)$. In addition, the values of S_j and A_j are set to be zero. It could help the current population to increase and hence avoid optimal local alternatives.

Rule #6: Stopping rank—The CHIO is implemented in Rules 3 to 5 until the stop requirement has been fulfilled, usually in accordance with the maximum number of iterations (Max_Itr). The total amount of protected and susceptible cases in this condition

dominates the population. The infected case will also be eliminated. The CHIO algorithm's flow diagram is shown in Figure 5.

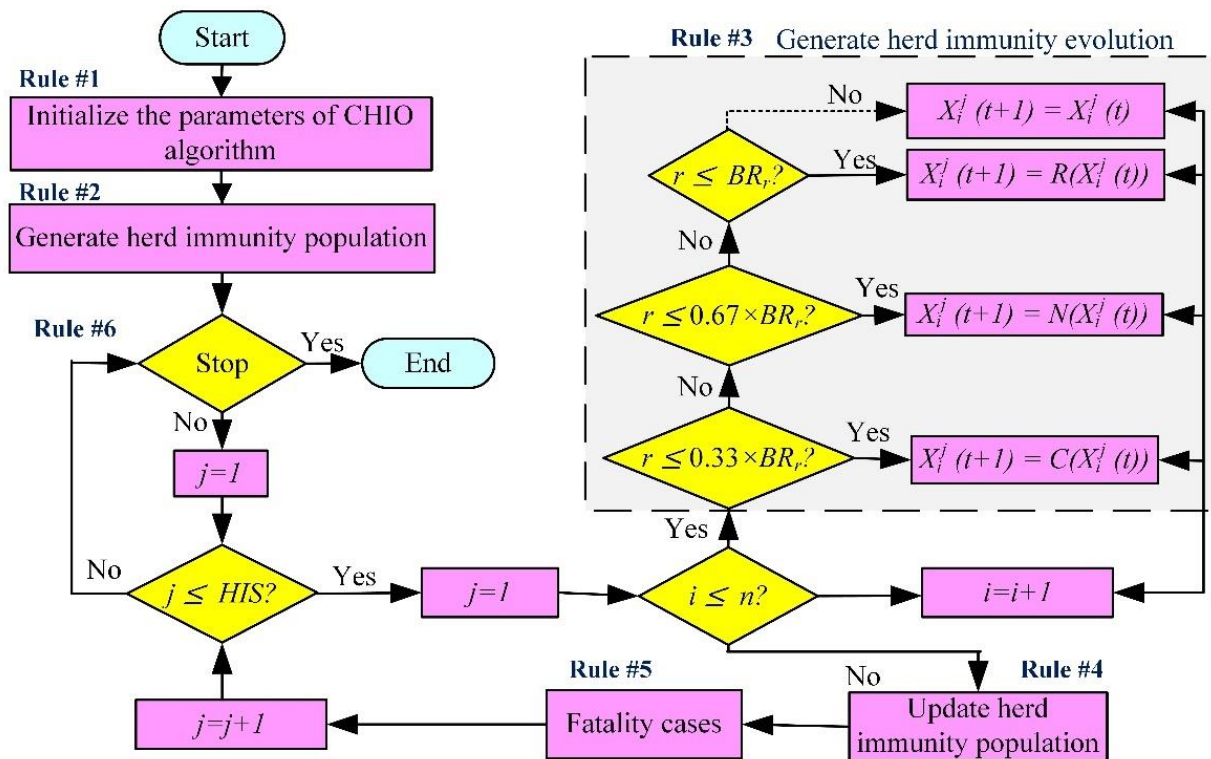


Figure 5. CHIO algorithm's flowchart [64].

4.1. Implementation Procedure of Multi-Objective CHIO

The implementation of the presented CHIO approach can be provided as follows.

1. Set the CHIO parameters; $Max_Itr = 300$; $Max_Age = 100$; popsize (HIS) = 50; $C_0 = 1$; $BR_r = 0.05$; lb and ub are given in each table in results.
2. Assess the immunological position of herd X using the Pareto sorting algorithm.
3. Obtain the non-dominated solution of the objective function as given in Equations (23), (25)–(28) together or individually, according to the implemented scenario.
4. Collect them in the Pareto archive and determine the crowding space for every archive member.
5. The Pareto sorting system is utilized for assessing the best person (non-dominated solution alone) in the archive, removing dominated alternatives from the archive.
6. The population located in the CHIO method is modernized with Equation (49).
7. Modernize the iteration cycle t to $t = t + 1$.
8. Return to Rule #2 if t is less than Max_Itr . The actual positions will be assessed and the ideal Pareto front S_I^X will be returned.
9. Find the best solutions for the Pareto sorting system.
10. Using a TOPSIS to obtain the one alternative that might be preferred through with the decision maker to speed up and integrate several possibilities as illustrated in the next Section 4.3.
11. In addition, we can use the AHP to obtain the weighting factors with the CHIO technique to transform MO into SO function 4.2.

4.2. Analytical Hierarchy Process

Once the variety of difficulties of engineering rises, because of the trade-offs, the single objective inquiry is no longer an excellent solution. Increasing the objective value

of a design may impair the performance of other objectives if several choices are offered. It can be utilized for multi-objective issues and techniques. However, several optimum spots on the Pareto graph that suit the criteria of decision makers three or four objectives, are not enough. This means that the decision maker might occasionally obtain one of Pareto’s most obvious questions to repeatedly look at all problems of interest. The AHP becomes one of the most often utilized techniques in decision making as well as provides numerous advantages among the multiple processes with various dimensions and features: simplicity, adjustability, and transparency that permit comparison and assessment of distinct possibilities. In the majority of cases, the main strategy to implementation of a priority setting is to discover the most viable solution [65].

The standard AHP procedure is summed up in [52]—building the model of hierarchal ranking; forming the judgment matrix; evaluating the maximum value of your own (λ_{max}), and the corresponding judgmental vector in which the elements of the vector reflect the relative factor weights and the “hierarchical ranking” and confirm the precision of the AHP with the consistency indices (CI) that should be less than 10%.

$$M = \begin{bmatrix} 1 & \psi_{12} & \psi_{13} & \psi_{14} \\ 1/\psi_{12} & 1 & \psi_{23} & \psi_{24} \\ 1/\psi_{13} & 1/\psi_{23} & 1 & \psi_{34} \\ 1/\psi_{14} & 1/\psi_{24} & 1/\psi_{34} & 1 \end{bmatrix}, \forall m, n \in N \tag{49}$$

where, $\psi_{mn} \in \{1, 3, 5, 7, 9\}$. N represents the number of the sub-objectives.

The consistency indices (CI) can be evaluated as follows:

$$CI = \frac{\lambda_{max} - N_j}{N_j - 1} \tag{50}$$

It can also evaluate the consistency ratio (CR), as the following:

$$CR = \frac{CI}{RI} \tag{51}$$

N_j and RI signify the judgment matrix dimension and the average random index, respectively. For further information about the AHP, please see [66–68].

The objectives are set corresponding to their relevance for the decision maker in this circumstance. In Egypt, the quality of the voltage is the priority based on the perspective of the energy suppliers and should meet national regulations. The main aim for network operators is to reduce fuel costs in the present period. The secondary objective is active power loss minimization. They are the third priority, notwithstanding the significance of reducing pollution levels.

The objective functions cannot be immediately merged into the solution due to their differing dimensions. As a result, the objective functions were normalized as follows:

$$\min_x \left(w_1 \frac{J_1(x)}{J_{10}} + w_2 \frac{J_2(x)}{J_{20}} + w_3 \frac{J_3(x)}{J_{30}} + w_4 \frac{J_4(x)}{J_{40}} + w_5 \frac{J_5(x)}{J_{50}} \right) \tag{52}$$

where $J_{10}, J_{20}, J_{30}, J_{40}$, and J_{50} represent the designer threshold values of the objective functions (maximum values). w_1, w_2, w_3, w_4 , and w_5 are the weighting factors of fuel costs, emissions, VD, P_{loss} , and $L-index$, respectively. Then, the weights are calculated as follows:

$$\varphi_m = \sum_{n=1}^{NF} \psi_{mn}, \forall m, n = 1, 2, 3, 4 \tag{53}$$

$$w_m = \frac{\varphi_m}{\sum_{n=1}^N \varphi_n} \tag{54}$$

In this work, the objective functions for Scenarios from 6 to 13 in the IEEE 30-bus system and for Scenarios 15 and 16 in the IEEE 57-bus are implemented using the AHP. Table 6 illustrates the judgment matrix and the weights of the EETD problem.

Table 6. The judgment matrix and the weights.

System	Scenario	Judgment Matrix (M)	Weights
IEEE 30-bus	6	$M = \begin{bmatrix} 1 & 2 \\ 0.5 & 1 \end{bmatrix}$	$w_1 = 0.6667$ $w_2 = 0.3333$
	7	$M = \begin{bmatrix} 1 & 2 \\ 0.5 & 1 \end{bmatrix}$	$w_1 = 0.6667$ $w_3 = 0.3333$
	8	$M = \begin{bmatrix} 1 & 2 \\ 0.5 & 1 \end{bmatrix}$	$w_1 = 0.6667$ $w_5 = 0.3333$
	9	$M = \begin{bmatrix} 1 & 2 & 2 \\ 0.5 & 1 & 1 \\ 0.5 & 1 & 1 \end{bmatrix}$	$w_1 = 0.5$ $w_3 = 0.25$ $w_4 = 0.25$
	10	$M = \begin{bmatrix} 1 & 2 & 2 \\ 0.5 & 1 & 3 \\ 0.5 & 0.33 & 1 \end{bmatrix}$	$w_1 = 0.44118$ $w_2 = 0.39706$ $w_4 = 0.16176$
	11	$M = \begin{bmatrix} 1 & 2 & 2 \\ 0.5 & 1 & 3 \\ 0.5 & 0.33 & 1 \end{bmatrix}$	$w_1 = 0.44118$ $w_2 = 0.39706$ $w_3 = 0.16176$
	12	$M = \begin{bmatrix} 1 & 2 & 2 & 2 \\ 0.5 & 1 & 1 & 3 \\ 0.5 & 1 & 1 & 3 \\ 0.5 & 0.3 & 0.3 & 1 \end{bmatrix}$	$w_1 = 0.34711$ $w_2 = 0.27273$ $w_3 = 0.27273$ $w_4 = 0.10744$
	13	$M = \begin{bmatrix} 1 & 2 & 2 & 2 & 2 \\ 0.5 & 1 & 1 & 1 & 3 \\ 0.5 & 1 & 1 & 1 & 3 \\ 0.5 & 1 & 1 & 1 & 3 \\ 0.5 & 0.3 & 0.3 & 0.3 & 1 \end{bmatrix}$	$w_1 = 0.29032$ $w_2 = 0.20968$ $w_3 = 0.20968$ $w_4 = 0.20968$ $w_5 = 0.080642$
IEEE 57-bus	15	$M = \begin{bmatrix} 1 & 2 \\ 0.5 & 1 \end{bmatrix}$	$w_1 = 0.6667$ $w_3 = 0.3333$
	16	$M = \begin{bmatrix} 1 & 2 \\ 0.5 & 1 \end{bmatrix}$	$w_1 = 0.6667$ $w_2 = 0.3333$

In progression, the judgment matrix and the weights are identified in this study, as illustrated in Table 6.

4.3. A Technique for Order Preference by Similarity to Ideal Solution

To compare Pareto with the optimization methods, just one alternative might be preferred through the decision maker to speed up and integrate several possibilities. Ranking or classification processes can be utilized to provide several non-dominant solutions. This work uses a classified approach called TOPSIS to resolve this variance in decision making with multi-attributes decision making (MADM) [69].

A TOPSIS manages to realize the best alternative that should include the quickest time from the positive-ideal alternative and the farthest time from the negative-ideal alternative. The major purpose of using a TOPSIS is to make computations coherent, understandable, and straightforward. The positive solution from all the best attributes and the negative alternative from all the worst attributes are generated by this procedure. A TOPSIS works

based on euclidean space computation to the ideal alternative [13]. The TOPSIS approach was used to classify the specific Pareto solutions achieved by the optimizations utilized. The primary premise of a TOPSIS is to discover an alternative that should be the smallest possible length from the ideal positive solution (\mathcal{H}^+) and the longest from the ideal negative alternative (\mathcal{H}^-).

In this study, the most important and smallest index change is the positive ideal solution (\mathcal{H}_{ij}^+), while the opposite solution is the negative ideal solution (\mathcal{H}_{ij}^-). The TOPSIS method is synthesized in these steps:

Rule #1: Define a decision matrix X . The value F_{ij} denotes a hint for the performing ranking of the i th choice regarding the j th function. Let, $S = (s_1, s_2)$ be the relative weighted trajectory of the objectives, fulfilling $\sum_{j=1}^n s_j = 1$.

Rule #2: Define the normalized value Z_{ij} by employing Equation (55):

$$Z_{ij} = \frac{F_{ij}}{\sqrt{\sum_{i=2}^n F_{ij}^2}} \forall i = 1, 2, \dots, n \ \& \ j = 1, 2 \tag{55}$$

Rule #3: Determine M_{ij} applying Equation (56) that signifies the weighted normalized decision matrix.

$$M_{ij} = s_j \times Z_{ij} \forall i = 1, 2, \dots, n \ \& \ j = 1, 2 \tag{56}$$

Rule #4: Obtain \mathcal{H}_{ij}^+ and \mathcal{H}_{ij}^- using Equations (57) and (58):

$$\mathcal{H}_{ij}^+ = \{\min(M_{11}, \dots, M_{n1}), \min(M_{12}, \dots, M_{n2})\} \tag{57}$$

$$\mathcal{H}_{ij}^- = \{\max(M_{11}, \dots, M_{n1}), \max(M_{12}, \dots, M_{n2})\} \tag{58}$$

Rule #5: Utilizing the n -dimensional euclidean space, define the split procedures through Equations (59) and (60):

$$S_{ij}^+ = \sqrt{\sum_{i=2}^n (M_{ij} - \mathcal{H}_{ij}^+)^2} \forall i = 1, 2, \dots, n \ \& \ j = 1, 2 \tag{59}$$

$$S_{ij}^- = \sqrt{\sum_{i=2}^n (M_{ij} - \mathcal{H}_{ij}^-)^2} \forall i = 1, 2, \dots, n \ \& \ j = 1, 2 \tag{60}$$

Rule #6: Evaluate the relative closeness (RC) to the ideal solution, which can be expressed as in Equation (61):

$$RC_{ij} = \frac{S_{ij}^-}{S_{ij}^+ + S_{ij}^-} \forall i = 1, 2, \dots, n \ \& \ j = 1, 2 \tag{61}$$

Rule #7: The preference order is to be rated so that the best compromise alternative can be considered as the alternative with the ultimate RC to the ideal alternative. Figure 6 shows the AHP implementation flowchart.

4.4. Implementation Procedure of EETD Problem

The implementation of the presented algorithms, including the AHP and the TOPSIS, can be summarized as follows:

1. Set the input data of TPGs and RESs; WP, PV, and PVTP as given in Table 3 in addition to the parameters of RESs.
2. Load the test systems of IEEE 30-bus and IEEE 57-bus from MATPOWER in Matlab.
3. Formulate the objective functions for SOEETD and MOEETD problems.
4. The AHP is employed with the MOEETD problem to obtain the weighting factors.
5. Set the algorithm's parameters—maximum number of iterations, search agents, ... etc.

6. Assess the decision variables; the active powers and voltage profiles buses, as illustrated in Tables A3 and A4.
7. Set the system constraints, as illustrated in Section 3.6.
8. Obtain the non-dominated solutions of the OFs.
9. Use a TOPSIS to obtain the best solution from the Pareto sorting system.

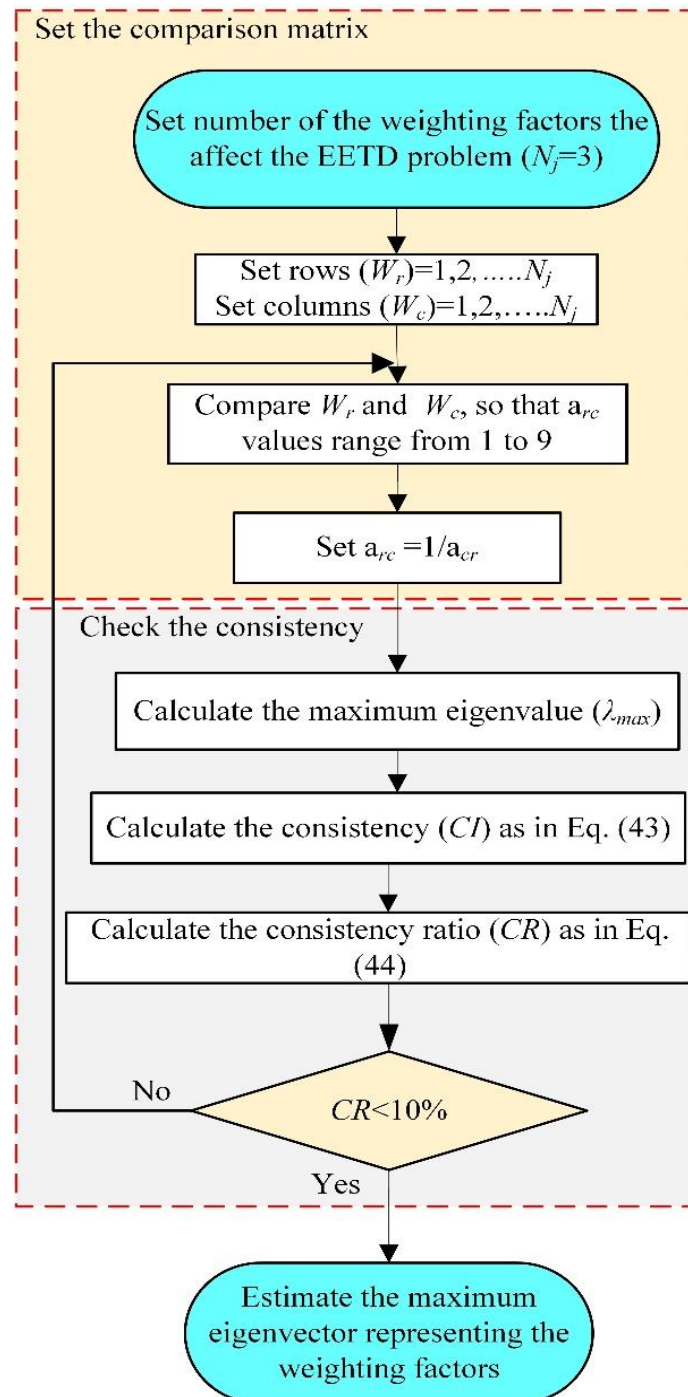


Figure 6. The AHP implementation flowchart.

The implementation of the presented algorithms, including the AHP and the TOPSIS, are depicted in Figure 7.

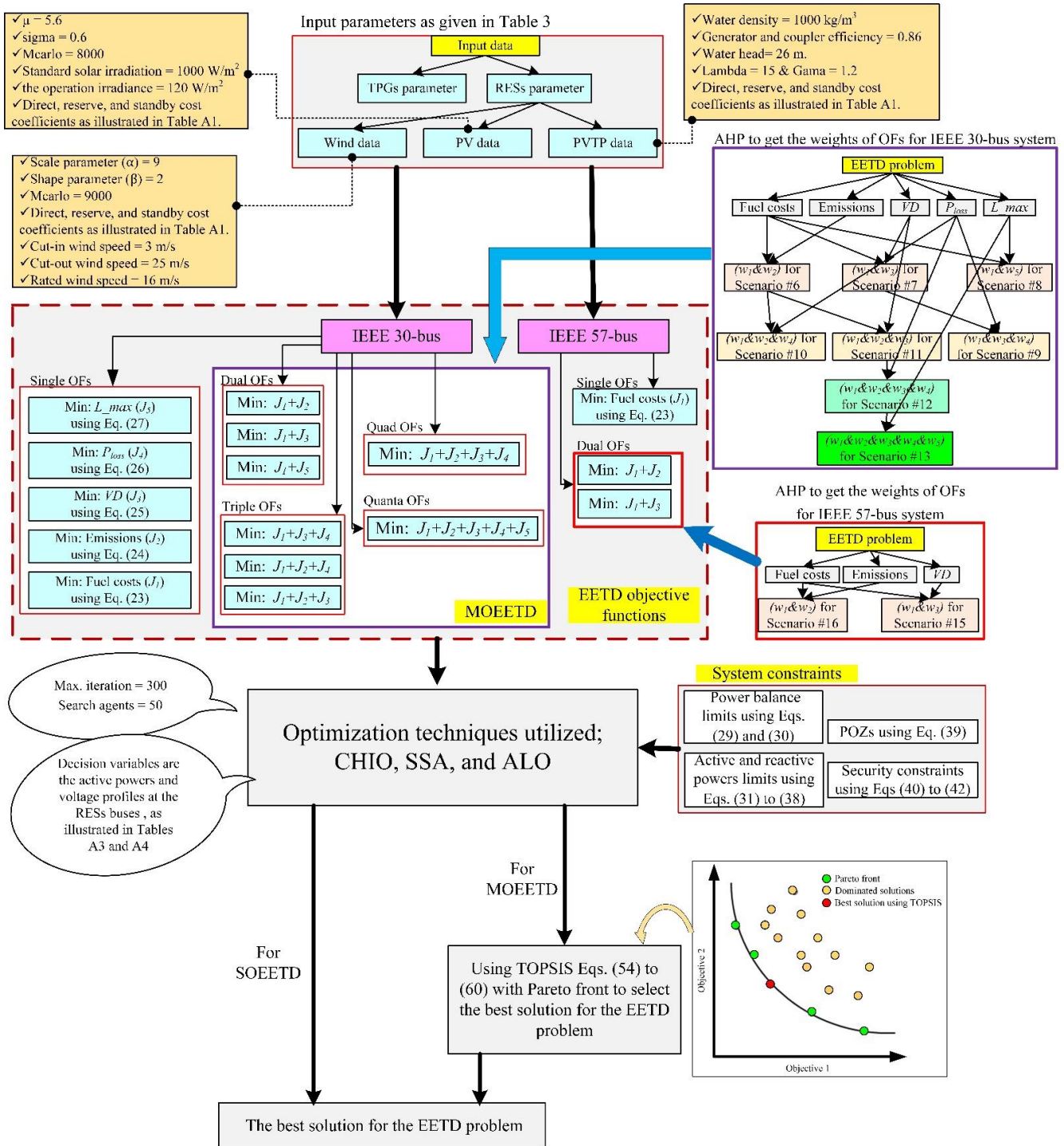


Figure 7. The implementation procedure of the EETD problem, including AHP and TOPSIS, techniques.

5. Results and Discussion

5.1. Results of IEEE 30-Bus Scheme

For SO and MO scenarios for this test scheme, the simulation findings are stated as follows:

5.1.1. Single Objective Scenarios

Tables 7 and 8 outline the details of the EETD simulation of Scenarios 1–5 with the three competitive optimization techniques: the CHIO, the ALO, and the SSA. It can be

noted, as shown in Table 7, that the lower and upper bounds are presented in the third and fourth columns. For instance, control variables are scheduled for Scenarios 1–3. The primary SOEETD utilizing three mentioned optimization approaches (in bold for each case) and the remaining objectives are described in Table 8.

Table 7. Lists of control variables for Scenarios 1–3 for IEEE 30-bus test scheme.

Variables and Parameters	Bounds		Scenario #1			Scenario #2			Scenario #3			
	Min	Max	CHIO	ALO	SSA	CHIO	ALO	SSA	CHIO	ALO	SSA	
Active power (MW)	P_{TPG2}	20	80	37.445	38.257	37.622	46.634	46.634	46.634	80	53.655	60.324
	P_{TPG5}	10	60	38.714	38.588	37.862	60	58.316	59.684	60	56.919	57.537
	P_{TPG8}	10	35	10	10	10	35	35	35	35	28.991	34.084
	P_{TPG11}	10	60	40.571	38.336	41.687	56.043	59.536	59.257	29.748	57.191	55.194
	P_{TPG13}	10	60	31.952	32.236	32.339	48.609	47.19	47.433	10	17.146	10.21
Reactive power (MVar)	Q_2	−20	60	10.108	21.867	−20	60	−6.6963	−20	−20	−20	−20
	Q_5	−30	35	35	26.714	35	−30	35	−1.7046	35	35	35
	Q_8	−15	40	40	40	40	40	−15	−5.0345	40	40	40
	Q_{11}	−25	30	18.137	18.382	21.412	−6.3482	2.2441	7.1202	36.844	39.512	39.207
	Q_{13}	−20	25	22.986	22.671	21.227	10.918	25	25	47.752	46.565	47.449
Bus voltage (pu)	V_1	0.96	1.10	1.1	1.1	1.1	1.1	1.0905	1.0729	1.0489	1.0438	0.99822
	V_2	0.96	1.10	1.09	1.0918	0.99286	1.1	1.0567	0.95162	0.95	1.0384	0.99455
	V_5	0.96	1.10	1.1	1.0722	1.0994	0.95	1.0876	0.96103	1.1	1.0993	1.093
	V_8	0.96	1.10	1.1	1.097	1.0971	1.0918	0.95844	0.96006	1.0877	1.0927	1.0904
	V_{11}	0.96	1.10	1.1	1.1	1.0991	0.96502	0.9741	0.95096	1.1	1.1	1.1
	V_{13}	0.96	1.10	1.1	1.0986	1.0872	1.0163	1.0434	1.0124	1.1	1.0973	1.098
$W_{\text{gen cost}}$			115.61	115.21	112.91	194.56	187.67	193.26	194.56	182.03	184.52	
$PV_{\text{gen cost}}$			109.11	102.45	112.92	164.93	179.01	177.89	80.349	169.75	162.67	
$PVTP_{\text{gen cost}}$			96.688	97.618	97.898	156.65	151.05	152.23	48.433	59.953	49.051	
$Fuel_{\text{vl cost}}$			447.542	454.04	445.92	332.75	332.76	332.75	543.67	414.62	456.16	
Fuel costs (\$/h)		Not applicable	768.95	769.32	769.64	848.89	850.48	856.14	867.01	826.36	852.4	
VD (pu)			1.1341	1.1054	0.90473	0.74422	0.83431	1.5518	0.36824	0.3779	0.3717	
P_{loss} (MW)			5.54	5.6165	5.6392	4.2397	4.6292	5.9627	4.4902	3.9095	4.0356	
L -index			0.11186	0.11316	0.12337	0.18187	0.19684	0.2305	0.07990	0.0799	0.0789	
Emissions (ton/h)			0.15187	0.15363	0.15086	0.09055	0.09055	0.09055	0.10619	0.0987	0.0988	
Computation time (s)			367.206	346.553	417.9415	361.393	413.8874	378.9375	538.9653	55.1077	465.364	

Table 8. Results of SOEETD problem using three optimization techniques for IEEE 30-bus (Scenarios 1–5).

Scenarios	Optimizations	Fuel costs (\$/h)	Emissions (ton/h)	VD (pu)	P_{loss} (MW)	L -Index
Scenario #1	CHIO	768.95	0.15187	1.1341	5.54	0.11186
	ALO	769.32	0.15363	1.1054	5.6165	0.11316
	SSA	769.64	0.15086	0.90473	5.6392	0.12337
Scenario #2	CHIO	848.89	0.09055	0.74422	4.2397	0.18187
	ALO	850.48	0.09055	0.83431	4.6292	0.19684
	SSA	856.14	0.09055	1.5518	5.9627	0.2305
Scenario #3	CHIO	867.01	0.10619	0.36824	4.4902	0.07990
	ALO	826.36	0.0987	0.3779	3.9095	0.0799
	SSA	852.4	0.0988	0.3717	4.0356	0.0789
Scenario #4	CHIO	895.88	0.10281	1.3265	2.0661	0.1013
	ALO	911.08	0.10922	1.3251	2.0724	0.10073
	SSA	872.76	0.095233	1.322	2.0848	0.10155
Scenario #5	CHIO	911.81	0.10833	0.4257	2.6828	0.071587
	ALO	913.04	0.10822	0.42521	2.6832	0.071614
	SSA	911.05	0.10792	0.42566	2.667	0.071596

In Scenario 1, minimization of the fuel costs is the major objective function (OF). The proposed CHIO technique offers the lowest cost (USD 768.95/h) compared with USD 769.32/h, USD 769.64/h obtained by ALO and SSA, respectively. In Scenario 2, minimization of the emission levels is the main OF. The proposed techniques: the CHIO, the ALO, and the SSA have achieved the minimum emission levels (0.09055 ton/h) that comply with environmental aspects. In Scenario 3, minimization of the VD is the main OF. The proposed CHIO technique has the least voltage deviation (0.36824 pu). In comparison to ALO and SSA techniques, the presented CHIO offers an improved voltage profile. In Scenario 4,

minimization of the P_{loss} is the main OF. The power losses are decreased by the presented approaches, the CHIO, the ALO, and the SSA, and their estimates become 2.0661 MW, 2.0724 MW, and 2.0848 MW, respectively. In Scenario 5, the L -index is minimized for improving the system stability. The quantities of L -index of the presented optimization approaches, the CHIO, the ALO, and the SSA equal 0.071587, 0.071614, and 0.071596, respectively.

Notably, the proposed CHIO indicates the best power loss reduction 2.0661 MW, the most economical alternative USD 768.95/h, and the improved voltage profile ($VD = 0.36824$ pu). In addition, the CHIO tends to have the least voltage stability index 0.071587 pu and emission levels 0.09055 ton/h. Figure 8 displays the convergence curves of the CHIO, the ALO, and the SSA techniques over several test schemes. These records illustrate that the CHIO influences the best values of the OF in the least number of iterations, consistently: for all test scenarios (1–5), the CHIO reaches the lowest OFs in comparison with the other methods in a smaller number of iterations, which proves the effectiveness of the presented technique.

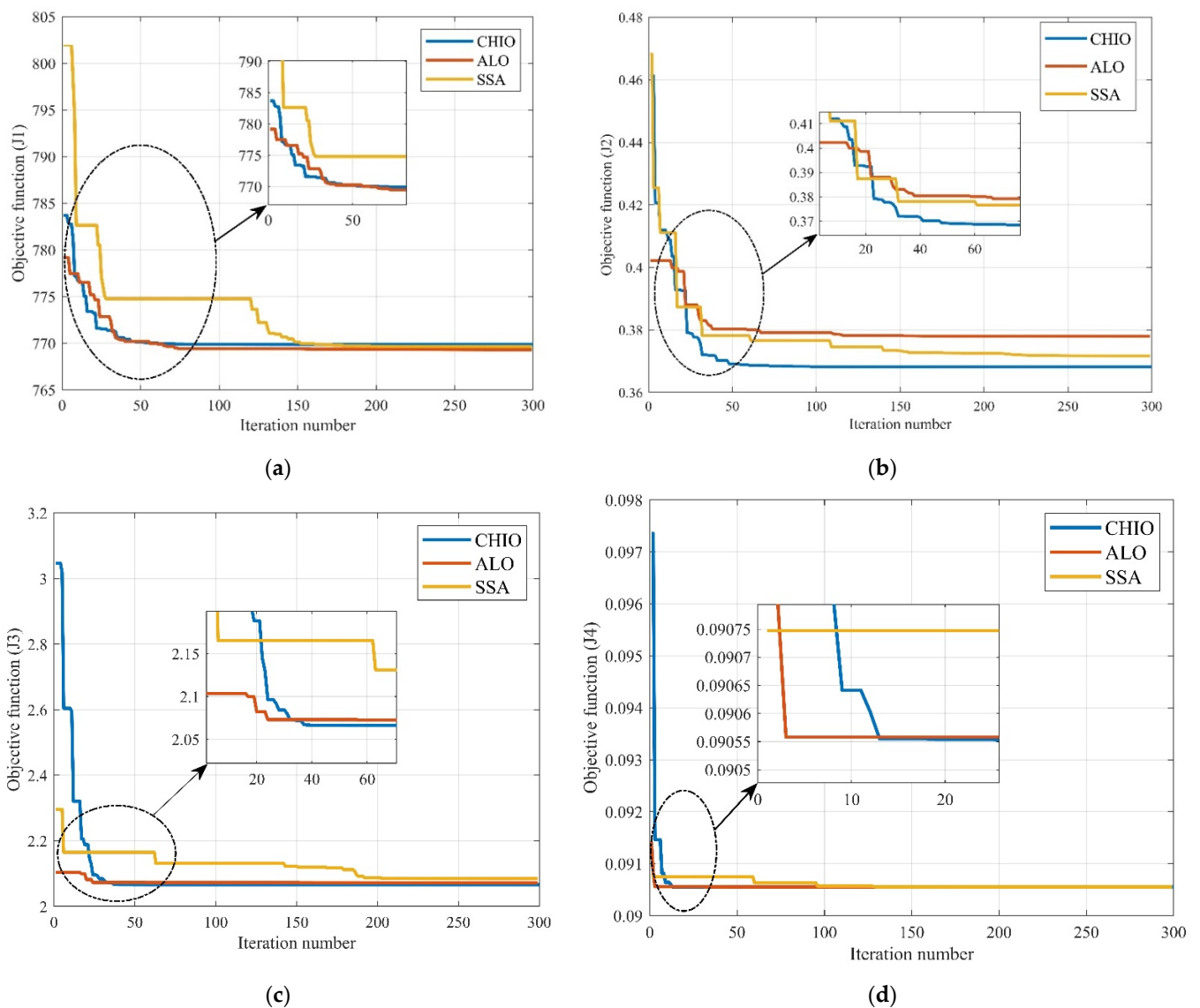


Figure 8. Cont.

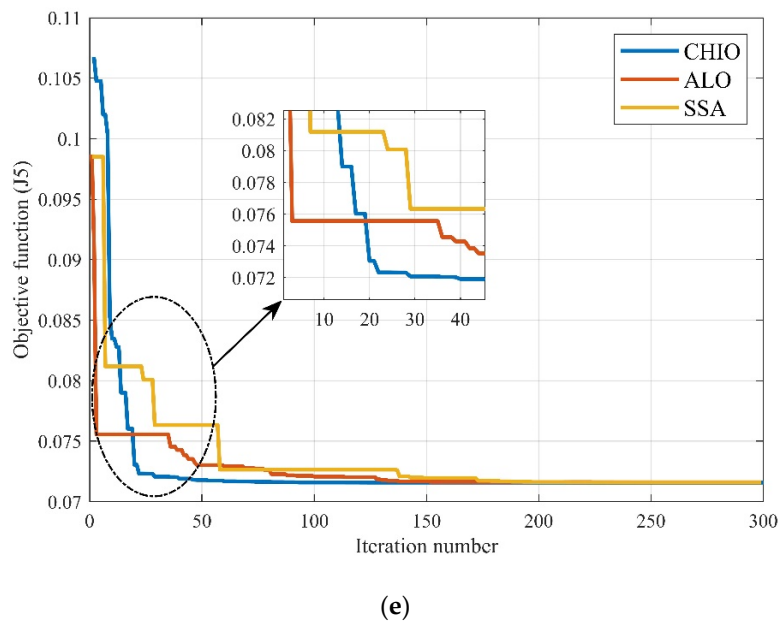


Figure 8. Convergence rates for Scenarios 1, 2, 3, 4, and 5 with CHIO, ALO, and SSA: (a) convergence rates for Scenario 1; (b) convergence rates for Scenario 2; (c) convergence rates for Scenario 3; (d) convergence rates for Scenario 4; (e) convergence rates for Scenario 5.

The proposed CHIO compared with the reported methods for Scenarios 1–5 is given in Table 9. In comparison to the literature approaches, the proposed CHIO contributes to competitiveness strategy for different scenarios (1–5).

Table 9. Comparative analysis for SO functions for IEEE 30-bus test scheme (Scenarios 1–5) (The numbers in bold are the best values found).

Scenarios	Scenario #1	Scenario #2	Scenario #3	Scenario #4	Scenario #5
IGWO [52]	811.838	0.09783	-	2.3584	-
DA-PSO [37]	802.12	0.205	-	3.189	-
MOALO [70]	799.14	-	-	-	-
MODA [71]	802.32	-	-	-	-
WOA-PS [71]	799.56	0.206	-	2.967	-
PSO-SSO [72]	798.98	0.205	1.25	2.858	0.124
ECBO [73]	799.035	-	-	-	-
ECHT [36]	800.41	0.205	-	3.084	0.136
DA-APSO [74]	802.63	-	-	3.003	-
MVO [75]	799.24	-	-	2.881	0.115
ALO	769.32	0.090553	0.37794	2.0724	0.071614
SSA	769.64	0.090553	0.37173	2.0848	0.071596
CHIO	768.95	0.090550	0.36824	2.0661	0.071587

5.1.2. Dual-Objective Scenarios

Tables 10 and 11 represent the scheduling of control variables and the simulation results of dual-objective scenarios (Scenarios 6–8) using the AHP, respectively. Scenario 6 enhances the fuel and emissions of generation stations concurrently. Scenario 7 enhances fuel costs and VD , while Scenario 8 reflects the fuel costs and the stability enhancement as the main dual-objective. The presented CHIO indicates the best compromise alternatives for Scenarios 6–8. The findings obtained the success of the presented CHIO compared to the literary methods mentioned. Figure 9 shows the efficacy of the CHIO technique proposed as opposed to the other algorithms SSA and ALO using the AHP technique.

Table 10. Lists of control variables for Scenarios 6–8 for IEEE 30-bus test scheme: AHP-based solutions (The numbers in bold are the best values found).

Variables and Parameters		Bounds		Scenario #6			Scenario #7			Scenario #8		
		Min	Max	CHIO	ALO	SSA	CHIO	ALO	SSA	CHIO	ALO	SSA
Active power (MW)	P_{TPG2}	20	80	36.731	36.279	38.165	37.265	36.304	38.277	37.393	37.786	37.368
	P_{TPG5}	10	60	38.259	39.366	38.253	38.639	39.291	38.74	38.683	38.721	39.174
	P_{TPG8}	10	35	10	10.001	10.794	10	10	10	10	10	10
	P_{TPG11}	0	60	43.679	42.398	38.918	40.932	42.481	43.261	40.947	37.993	36.702
	P_{TPG13}	10	60	32.958	31.971	32.57	32.446	31.727	31.403	31.862	32.205	33.668
Reactive power (MVar)	Q_2	-20	60	10.833	10.874	9.6167	18.225	11.811	-20	11.203	11.39	19.449
	Q_5	-30	35	35	35	35	24.834	35	35	35	35	26.742
	Q_8	-15	40	40	40	40	40	40	40	40	40	40
	Q_{11}	-25	30	19.086	18.154	18.192	21.655	19.127	22.201	18.895	18.226	19.549
	Q_{13}	-20	25	19.924	22.768	22.559	14.549	16.545	19.504	20.235	22.113	19.33
Bus voltage (pu)	V_1	0.96	1.10	1.1	1.1	1.1	1.1	1.1	1.1	1.1	1.1	1.1
	V_2	0.96	1.10	1.0899	1.0905	1.0897	1.0879	1.089	0.9585	1.0899	1.0901	1.09
	V_5	0.96	1.10	1.1	1.0996	1.0894	1.0655	1.1	1.0985	1.1	1.0993	1.0702
	V_8	0.96	1.10	1.1	1.0999	1.0769	1.1	1.0874	1.0692	1.1	1.0955	1.0763
	V_{11}	0.96	1.10	1.1	1.1	1.1	1.1	1.0966	1.1	1.1	1.1	1.1
	V_{13}	0.96	1.10	1.0913	1.0997	1.0987	1.0721	1.0798	1.0823	1.0919	1.0975	1.088
$W_{\text{gen cost}}$			114.16	117.71	114.14	115.37	117.47	115.7	115.51	115.63	117.09	
$PV_{\text{gen cost}}$			119.65	115.73	104.92	110.19	115.64	118.66	110.68	101.58	98.182	
$PVTP_{\text{gen cost}}$			99.824	96.776	98.611	98.248	96.042	95.024	96.568	97.476	102.11	
$Fuel_{\text{lv cost}}$			436.16	439.69	452.51	445.08	440.45	441.12	446.73	454.86	452.84	
Fuel costs (\$/h)		Not applicable	769.79	769.91	770.19	768.89	769.6	770.5	769.49	769.55	770.22	
VD (pu)			1.0767	1.1414	1.1208	0.87394	0.96677	0.88008	1.0753	1.1121	1.0101	
P_{loss} (MW)			5.3788	5.4231	5.5705	5.4964	5.4415	5.5104	5.5244	5.6632	5.627	
L -index			0.11387	0.11146	0.11234	0.12229	0.1179	0.12414	0.11259	0.11388	0.11691	
Emissions (ton/h)			0.1478	0.15006	0.15161	0.15101	0.15036	0.14771	0.15158	0.15475	0.15446	
Execution time (s)			385.0354	353.1225	384.7674	343.9965	348.5127	430.5964	309.6968	408.3730	391.4846	

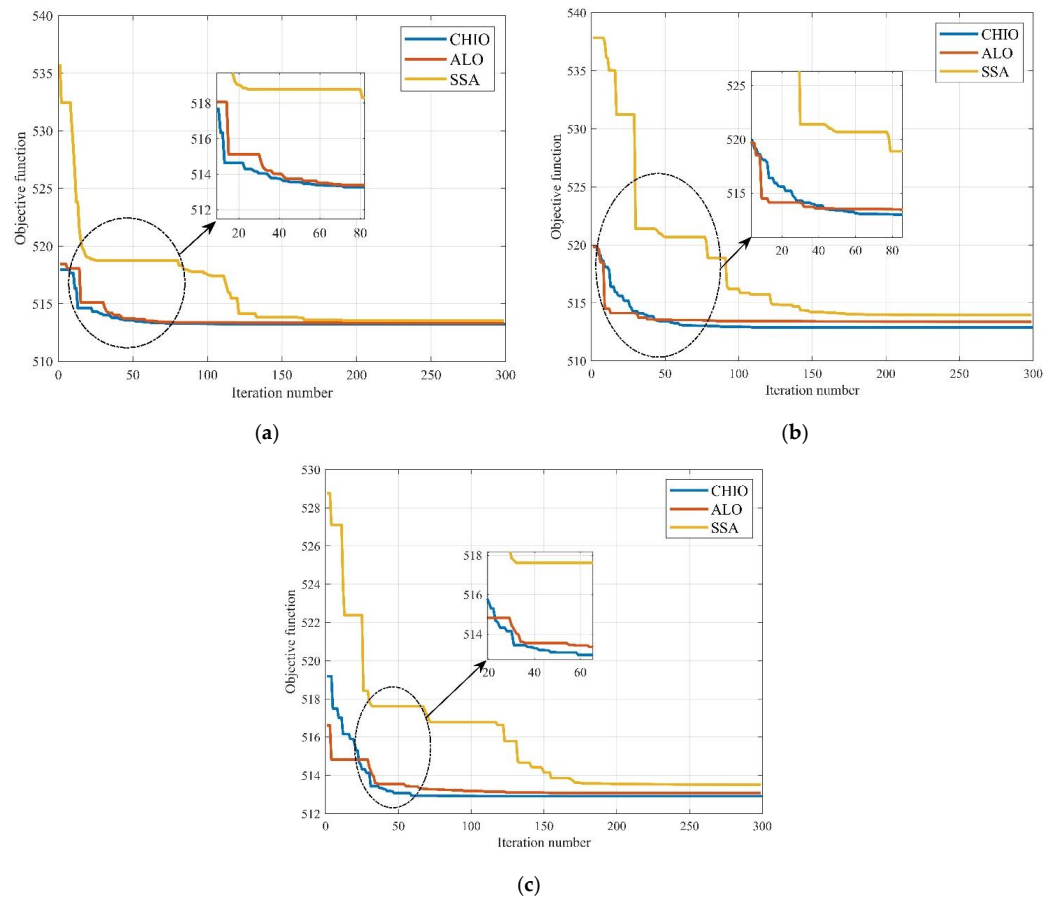


Figure 9. Convergence rates for Scenarios 6, 7, and 8 with CHIO, ALO, and SSA: (a) convergence rates for Scenario #6; (b) convergence rates for Scenario 7; (c) convergence rates for Scenario 8.

Table 11. Numerical results of Scenarios 6–8 for IEEE 30-bus test scheme “Dual-objectives”.

Scenarios	Scenario #6			Scenario #7			Scenario #8		
Optimizations	CHIO	ALO	SSA	CHIO	ALO	SSA	CHIO	ALO	SSA
Fuel costs (\$/h)	769.79	769.91	770.19	768.89	769.6	770.5	769.49	769.55	770.22
Emissions (ton/h)	0.1478	0.1501	0.1516	0.1510	0.1504	0.1477	0.1516	0.1548	0.1545
VD (pu)	1.0767	1.1414	1.1208	0.8739	0.9668	0.8801	1.0753	1.1121	1.0101
P_{loss} (MW)	5.3788	5.4231	5.5705	5.4964	5.4415	5.5104	5.5244	5.6632	5.627
L-index	0.1139	0.1115	0.1123	0.1223	0.1179	0.1241	0.1139	0.1126	0.1169

Figure 10 explains the Pareto fronts with the strategies CHIO, ALO, and SSA for Scenarios 6–8. In Scenarios 6–8, Table 12 demonstrates the numerical results of the presented CHIO using TOPSIS in comparison with further utilized techniques. The use of the CHIO is more competitive in various scenarios relative to the approaches described.

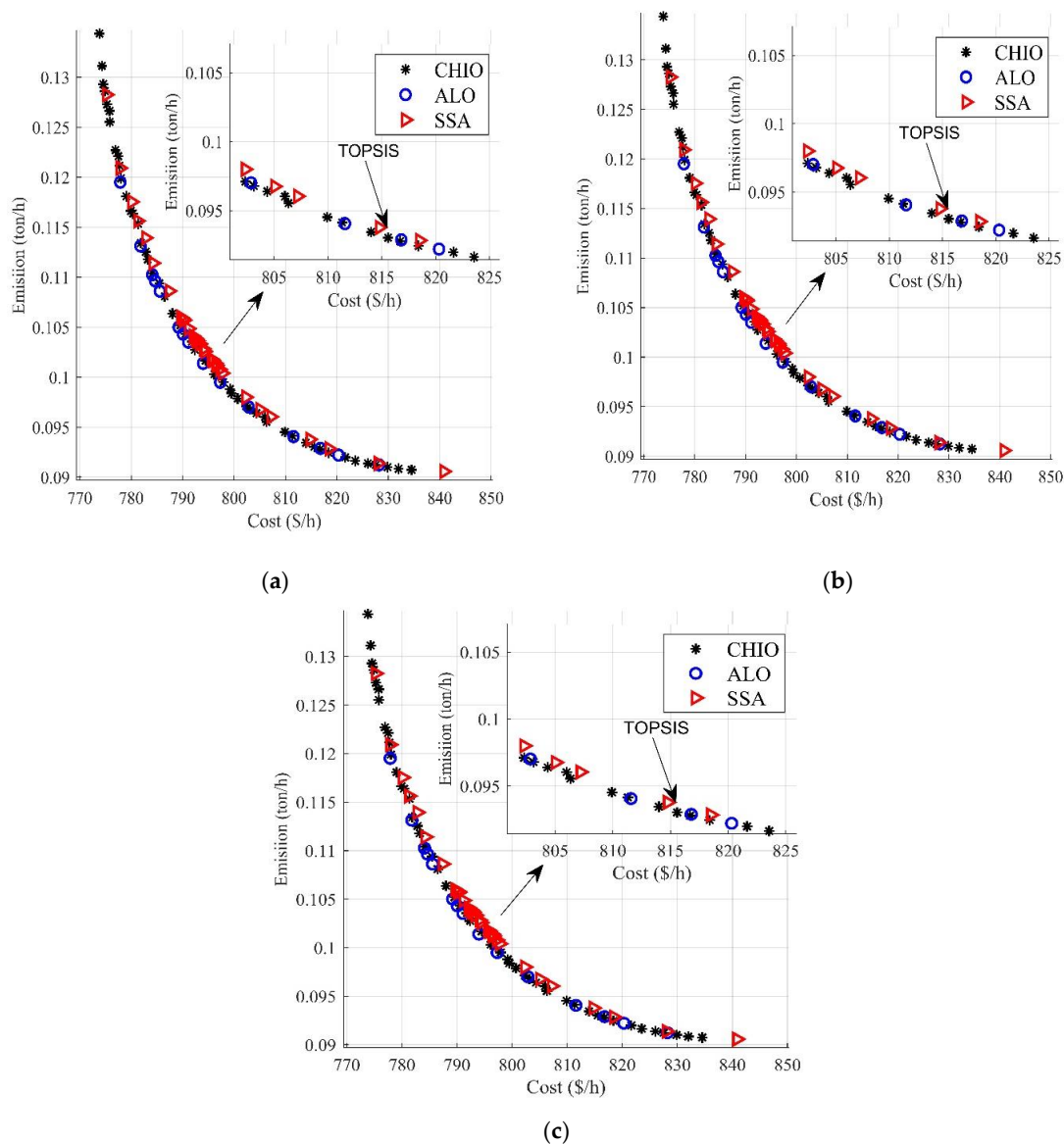


Figure 10. Pareto fronts with CHIO, ALO, and SSA for Scenario 6–8. (a) Pareto fronts with CHIO, ALO, and SSA for Scenario 6; (b) Pareto fronts with CHIO, ALO, and SSA for Scenario 7; (c) Pareto fronts with CHIO, ALO, and SSA for Scenario 8.

Table 12. Lists of control variables for Scenarios 6–8 for IEEE 30-bus test scheme: TOPSIS-based solutions (The numbers in bold are the best values found).

Variables and Parameters		Bounds		Scenario #6			Scenario #7			Scenario #8		
		Min	Max	CHIO	ALO	SSA	CHIO	ALO	SSA	CHIO	ALO	SSA
Active power (MW)	P_{TPG2}	0	80	47.845	48.982	46.078	45.621	40.152	66.178	39.117	47.489	42.04
	P_{TPG5}	10	60	49.719	53.164	51.233	24.064	55.8	40.281	42.978	42.409	45.261
	P_{TPG8}	10	35	33.338	29.341	30.902	22.187	31.809	26.5	30.152	33.634	34.153
	P_{TPG11}	0	60	54.086	54.074	54.865	38.309	42.535	39.127	45.717	55.79	44.429
	P_{TPG13}	10	60	41.396	42.335	44.852	20.455	18.392	21.337	36.454	36.587	41.89
Reactive power (MVar)	Q_2	-20	60	-19.618	12.779	-20	-20	-20	60	-20	-20	-20
	Q_5	-30	35	34.737	35	35	35	35	-17.095	35	35	35
	Q_8	-15	40	40	40	40	72.152	40	40	40	40	40
	Q_{11}	-25	30	20.212	15.917	11.242	31.598	38.362	30	43.473	39.702	38.295
	Q_{13}	-20	25	25	19.142	25	29.794	47.92	25	46.347	47.177	46.652
Bus voltage (pu)	V_1	0.96	1.10	1.0659	1.0995	1.0533	0.96637	1.0343	0.97412	1.0226	1.0384	0.99867
	V_2	0.96	1.10	1.052	1.0989	0.97869	0.97955	1.0103	1.0998	0.99434	1.019	0.96053
	V_5	0.96	1.10	1.0491	1.0989	1.0657	1.0446	1.0825	0.98497	1.0773	1.0997	1.0447
	V_8	0.96	1.10	1.0624	1.0995	1.0687	1.0366	1.0743	1.0966	1.0753	1.0985	1.0639
	V_{11}	0.96	1.10	1.0734	1.0988	1.0218	1.09	1.1	1.1	1.0962	1.1	1.1
	V_{13}	0.96	1.10	1.0808	1.0981	1.0548	1.0662	1.1	1.0963	1.0829	1.1	1.1
$W_{\text{gen cost}}$			154.01	167.18	159.74	75.685	177.55	120.69	129.76	127.81	137.73	
$PV_{\text{gen cost}}$			157.51	157.62	160.32	102.42	116.29	105.3	126.84	164.06	122.63	
$PVTP_{\text{gen cost}}$			128.89	132.48	141.83	66.546	62.286	68.505	111.31	111.82	130.62	
$Fuel_{\text{lv cost}}$			375.16	359.52	356.61	559.47	448.08	512.21	424.55	406.85	412.72	
Fuel costs (\$/h)			815.57	816.8	818.5	804.13	804.21	806.7	792.46	810.54	803.7	
VD (pu)	Not applicable		0.54468	1.3086	0.53194	0.37806	0.38057	0.39431	0.55733	0.39718	0.39866	
P_{loss} (MW)			3.086	2.7679	3.2697	8.0997	4.7286	5.3882	5.0538	4.1804	4.3633	
$L\text{-index}$			0.11179	0.1011	0.13014	0.088852	0.08199	0.1176	0.079419	0.08353	0.08072	
Emissions (ton/h)			0.092838	0.09288	0.09303	0.17045	0.11515	0.11512	0.11124	0.09741	0.10176	
Computation time (s)			1070.14	318.07	441.79	1260.03	403.06	501.39	1265.38	433.11	466.480	

An evaluation of the previous related studies for dual objectives was stated in Table 13. The results obtained the effectiveness of the presented CHIO compared to the literary methods mentioned. The results in bold are more competitive solutions using three optimization techniques.

Table 13. Comparative analysis for dual objective functions (Scenarios 6–8).

Scenarios	Scenario #6		Scenario #7		Scenario #8	
Objective Functions	Fuel Costs (\$/h)	Emissions (ton/h)	Fuel Costs (\$/h)	VD (pu)	Fuel Costs (\$/h)	L-Index
MOMICA [34]	865.06	0.222	804.96	0.095	-	-
MOFA-CPA [33]	852.02	0.279	-	-	-	-
MODA [37]	838.604	0.254	807.2807	0.023	-	-
PSO-SSO [72]	834.804	0.243	803.99	0.094	830.35	0.125
ECHT [36]	-	-	803.72	0.095	-	-
DA-APSO [74]	-	-	802.63	0.116	-	-
ALO	769.91	0.15006	769.6	0.96677	769.55	0.11388
SSA	770.19	0.15161	770.5	0.88008	770.22	0.11259
CHIO	769.79	0.1478	768.89	0.87394	769.49	0.11691

5.1.3. Triple-Objective Scenarios

Tables 14 and 15 display the outcomes of simulations obtained for three objective functions for the SSA, the ALO, and the proposed CHIO for Scenarios 9–11 using the AHP and the TOPSIS, respectively. In Scenario 9, three objectives are taken into account: fuel costs, power losses, and voltage deviation minimizations. In Scenario 10, fuel cost, P_{loss} , and carbon minimizations are considered. The fuel costs, voltage drop, and emission levels are considered in Scenario 11.

Table 14. Lists of control variables for Scenarios 9–11 for IEEE 30-bus test scheme: AHP-based solutions (The numbers in bold are the best values found).

Variables and Parameters		Bounds		Scenario #9			Scenario #10			Scenario #11		
		Min	Max	CHIO	ALO	SSA	CHIO	ALO	SSA	CHIO	ALO	SSA
Active power (MW)	P_{TPG2}	0	80	37.915	37.263	37.519	37.575	37.915	36.998	36.901	37.704	38.33
	P_{TPG5}	10	60	39.431	39.388	39.224	39.494	39.405	39.785	38.405	37.865	36.99
	P_{TPG8}	10	35	10	10	10	10	10	10.017	10	10	10.183
	P_{TPG11}	0	60	37.924	38.554	42.819	41.433	41.144	42.807	43.679	37.467	39.543
	P_{TPG13}	10	60	33.009	33.044	32.741	32.477	33.166	32.29	31.781	33.385	32.736
Reactive power (MVar)	Q_2	−20	60	18.253	19.472	16.951	17.964	18.299	18.561	18.407	16.73	17.025
	Q_5	−30	35	24.857	26.403	23.888	25.398	26.694	28.245	24.611	24.745	24.721
	Q_8	−15	40	40	40	40	40	40	40	40	40	40
	Q_{11}	−25	30	21.124	18.252	20.827	19.39	18.651	19.265	23.083	20.747	21.473
	Q_{13}	−20	25	15.705	19.236	17.916	21.272	22.718	20.103	10.631	16.58	14.895
Bus voltage (pu)	V_1	0.96	1.10	1.1	1.1	1.1	1.1	1.1	1.1	1.1	1.1	1.1
	V_2	0.96	1.10	1.0882	1.0896	1.0883	1.0899	1.0909	1.091	1.0871	1.0872	1.0871
	V_5	0.96	1.10	1.0661	1.0692	1.0658	1.0695	1.072	1.0734	1.0638	1.0646	1.064
	V_8	0.96	1.10	1.0995	1.099	1.0908	1.1	1.0988	1.0919	1.098	1.0784	1.0962
	V_{11}	0.96	1.10	1.1	1.0946	1.1	1.1	1.1	1.1	1.1	1.0986	1.0991
	V_{13}	0.96	1.10	1.0758	1.086	1.0824	1.0934	1.0985	1.0912	1.0597	1.0774	1.0723
$W_{\text{gen cost}}$			117.92	117.78	117.25	118.12	117.83	119.07	114.63	112.92	110.18	
$PV_{\text{gen cost}}$			101.29	102.96	117.07	112.26	112.23	116.7	119.65	100.3	105.73	
$PVTP_{\text{gen cost}}$			100.07	100.15	99.192	98.338	100.51	97.759	96.223	101.19	99.137	
$Fuel_{\text{vlvcost}}$			450.24	448.3	436.4	440.65	439.73	436.03	439.35	455.56	453.9	
Fuel costs (\$/h)		Not applicable	769.19	769.53	769.91	769.38	770.3	769.56	769.85	769.97	768.95	
VD (pu)			0.89865	0.96724	0.95242	1.0514	1.1035	1.0609	0.78891	0.88963	0.85853	
P_{loss} (MW)			5.5598	5.547	5.3219	5.3811	5.367	5.3112	5.4224	5.6972	5.6488	
L -index			0.12136	0.11871	0.11957	0.11559	0.11345	0.11468	0.1258	0.12208	0.1232	
Emissions (ton/h)			0.15239	0.1525	0.14674	0.14855	0.14763	0.14732	0.14897	0.15521	0.15312	
Execution time (s)			279.63	347.842	362.581	274.884	375.193	384.989	272.287	364.287	385.129	

Table 15. Lists of control variables for Scenarios 9–11 for IEEE 30-bus test scheme: TOPSIS-based solutions (The numbers in bold are the best values found).

Variables and Parameters		Bounds		Scenario #9			Scenario #10			Scenario #11		
		Min	Max	CHIO	ALO	SSA	CHIO	ALO	SSA	CHIO	ALO	SSA
Active power (MW)	P_{TPG2}	0	80	45.405	48.361	62.321	46.448	53.022	45.228	57.368	48.538	49.279
	P_{TPG5}	10	60	55.529	50.909	52.175	71.7	56.496	54.824	49.2	46.063	48.875
	P_{TPG8}	10	35	32.838	26.289	30.04	34.277	29.567	29.62	31.29	25.863	26.658
	P_{TPG11}	0	60	42.484	55.725	51.342	59.487	57.34	51.823	51.129	51.793	50.458
	P_{TPG13}	10	60	34.013	43.227	25.283	40.994	41.834	42.571	39.104	43.911	39.191
Reactive power (MVar)	Q_2	−20	60	−20	15.13	−20	13.944	−3.0635	−20	−20	−2.0587	32.849
	Q_5	−30	35	35	32.075	35	23.902	34.535	35	35	35	19.43
	Q_8	−15	40	40	40	40	40	40	40	33.567	40	40
	Q_{11}	−25	30	23.42	19.691	21.981	17.235	16.358	11.408	25.992	19.223	18.668
	Q_{13}	−20	25	18.363	12.202	25	19.746	18.545	18.641	24.103	21.071	25
Bus voltage (pu)	V_1	0.96	1.10	1.0745	1.0734	1.0649	1.095	1.0915	1.0813	1.0526	1.0631	1.0155
	V_2	0.96	1.10	1.0537	1.0697	1.0252	1.0947	1.0846	1.0137	0.96787	1.054	1.0201
	V_5	0.96	1.10	1.0716	1.0596	1.0815	1.0859	1.0813	1.0654	1.0569	1.0653	0.99491
	V_8	0.96	1.10	1.0651	1.0713	1.0763	1.0983	1.0869	1.0725	1.0326	1.0621	1.0204
	V_{11}	0.96	1.10	1.0899	1.0729	1.0787	1.097	1.0851	1.0479	1.0754	1.0661	1.025
	V_{13}	0.96	1.10	1.065	1.0468	1.0787	1.0955	1.0831	1.059	1.0594	1.0612	1.0585
$W_{\text{gen cost}}$			176.48	158.51	163.35	244.28	180.33	173.68	152.07	140.59	150.86	
$PV_{\text{gen cost}}$			115.16	163.95	147.25	177.97	169.19	148.74	146.02	149.08	143.64	
$PVTP_{\text{gen cost}}$			103.26	135.73	77.989	127.38	130.44	133.12	120.58	138.35	120.81	
$Fuel_{\text{vlvcost}}$			406.04	355.05	429.43	308.98	349.31	357.93	397.85	376.03	386.85	
Fuel costs (\$/h)		Not applicable	800.93	813.24	818.02	858.61	829.27	813.47	816.52	804.05	802.16	
VD (pu)			0.59367	0.50992	0.53133	1.2231	0.96821	0.48706	0.43323	0.46179	0.73504	
P_{loss} (MW)			3.3057	3.06	3.326	1.9072	2.5598	3.0963	3.2613	3.5004	3.7856	
L -index			0.11386	0.11634	0.11076	0.10076	0.10914	0.12837	0.11684	0.11521	0.12004	
Emissions (ton/h)			0.09912	0.09411	0.09662	0.091123	0.09144	0.09394	0.093589	0.09718	0.09799	
Computation time (s)			995.1156	318.7531	524.7601	1000.5954	302.5808	425.4336	1186.5667	322.3311	431.3868	

In Scenario 9, the proposed CHIO obtained the best fuel cost and voltage deviation, while the SSA technique achieved the best reduction in power losses. In Scenario 10, the proposed CHIO obtained the best economic benefit, while the SSA technique obtained the best reduction in power losses and environmental benefits. In Scenario 11, the proposed CHIO obtained the best values in all objectives of that scenario. Figure 11 indicates Pareto fronts with ALO, SSA, and the proposed CHIO methods for Scenarios 9–11.

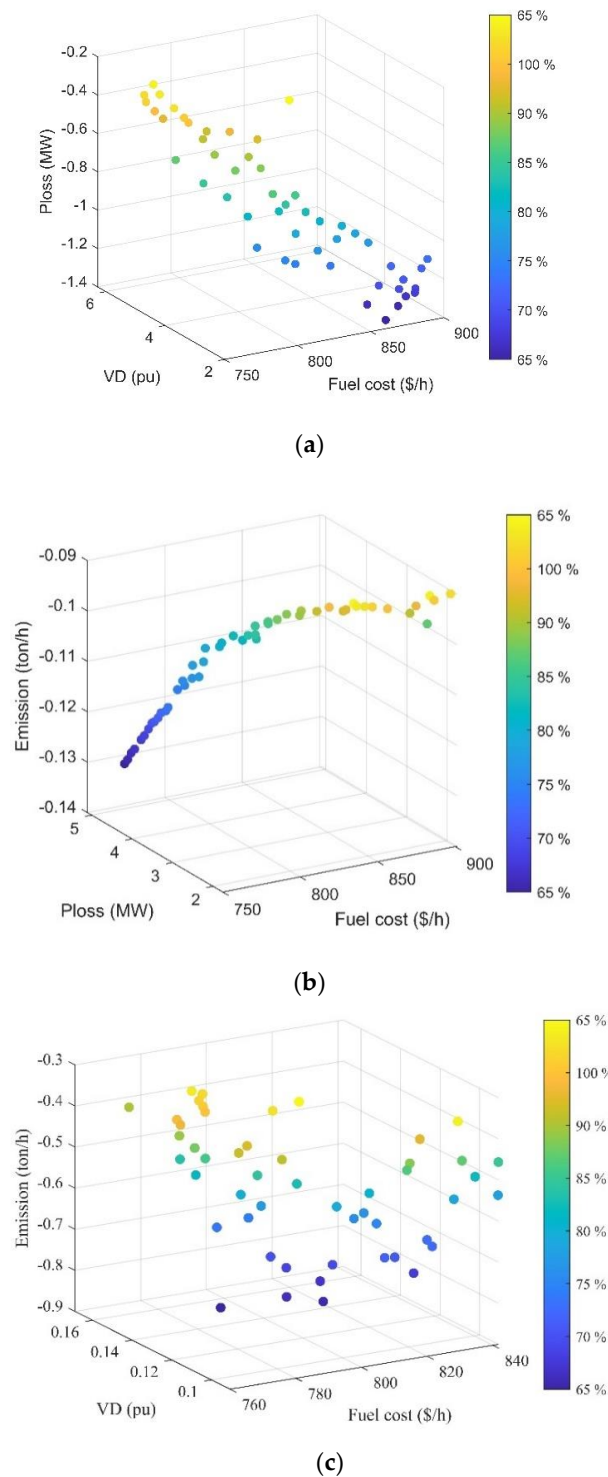


Figure 11. Pareto fronts with CHIO, ALO, and SSA for Scenarios 9–11: (a) Pareto fronts with CHIO, ALO, and SSA for Scenario 9; (b) Pareto fronts with CHIO, ALO, and SSA for Scenario 10; (c) Pareto fronts with CHIO, ALO, and SSA for Scenario 11.

The fuel costs in Scenarios 9, 10, and 11 obtained using the AHP are more economical than obtained using a TOPSIS. In Scenario 9, voltage deviation and power losses obtained using a TOPSIS are more technical than obtained using the AHP. In Scenario 10, emission levels and power losses obtained using a TOPSIS are more environmental and technical than obtained using the AHP, respectively. In addition, voltage deviation and emission levels obtained in Scenario 11 using a TOPSIS are more technical and offer more environ-

mental benefits than obtained using the AHP, respectively. To sum up, we can say that optimization techniques using the AHP are superior to obtaining the best values of fuel costs in comparison to the TOPSIS while the optimization techniques using the TOPSIS has more environmental and technical benefits in comparison to the AHP in the case of triple-objective scenarios.

An evaluation of the previous related studies for triple-objectives is stated in Table 16. The results obtained the effectiveness of the presented CHIO in comparison with the literary methods mentioned. The results in bold are more competitive solutions using three optimization techniques.

Table 16. Comparative analysis for triple-objective functions (Scenarios 9–11) (The numbers in bold are the best values found).

Scenarios Objective Functions	Scenario #9			Scenario #10			Scenario #11		
	Fuel Costs (\$/h)	VD (pu)	Power Losses (MW)	Fuel Costs (\$/h)	Emissions (ton/h)	Power Losses (MW)	Fuel Costs (\$/h)	Emissions (ton/h)	VD (pu)
MOFA-CPA [33]	-	-	-	878.13	0.2165	3.9232	-	-	-
MODA [37]	-	-	-	867.9070	0.2640	4.5342	-	-	-
PSO-SSO [72]	864.27	0.316	4.545	865.18	0.224	4.093	804.332	0.346	0.164
ALO	769.19	0.96724	5.547	770.3	0.14763	5.367	769.97	0.15521	0.88963
SSA	769.91	0.95242	5.3219	769.56	0.14732	5.3112	768.95	0.15312	0.85853
CHIO	769.53	0.89865	5.5598	769.38	0.14855	5.3811	769.85	0.14897	0.78891

5.1.4. Quad-Objective Scenario

Table 17 displays EETD simulation results for the quad objective “Scenario 12”. This table confirms that the presented CHIO leads, in comparison with the ALO and the SSA using the TOPSIS, to the most competitive economic solutions at tolerable voltages of system losses. The convergence curve in Figure 12 displays the efficiency and the minimum number of iterations of the proposed CHIO method using the AHP. Furthermore, Table 18 assesses the CHIO offered as compared to MOMICA [34], I-NSGA-III [35], MODA [37], and ECHT [36] in the context of Scenario 12 and individual ALO and SSA techniques. In comparison to existing individual optimization methods using the ALO and the SSA, the proposed CHIO approach offers the best possible compromise solution.

Table 17. Lists of control variables for Scenario 12 for IEEE 30-bus test scheme: TOPSIS-based solutions (The numbers in bold are the best values found).

Variables and Parameters	Min.	Max.	CHIO	ALO	SSA	
Active power (MW)	P_{TG2}	20	80	48.714	50.953	47.125
	P_{TG5}	10	60	48.81	54.609	50.637
	P_{TG8}	10	35	27.752	33.426	31.178
	P_{TG11}	10	60	54.453	48.113	54.953
	P_{TG13}	10	48.652	39.445	36.464	43.843
Reactive power (MVar)	Q_2	-20	60	33.559	6.7174	-20
	Q_5	-30	35	26.541	35	28.401
	Q_8	-15	40	40	38.79	40
	Q_{11}	-25	30	16.525	17.953	16.23
	Q_{13}	-20	25	14.031	14.739	12.23
Bus voltage (pu)	V_1	0.96	1.10	1.071	1.0769	1.0804
	V_2	0.96	1.10	1.0723	1.0716	0.99356
	V_5	0.96	1.10	1.0543	1.074	1.0452
	V_8	0.96	1.10	1.0697	1.0619	1.05
	V_{11}	0.96	1.10	1.0634	1.0759	1.0526
V_{13}	0.96	1.10	1.0499	1.0581	1.0363	

Table 17. Cont.

Variables and Parameters	Min.	Max.	CHIO	ALO	SSA
W_{gencost}			150.62	172.84	157.47
PV_{gencost}			159.28	134.89	160.63
$PVTP_{\text{gencost}}$			121.73	111.72	138.18
$Fuel_{\text{vlvcost}}$			375.46	392.93	361.45
Total cost (\$/h)			807.09	812.37	817.74
VD (pu)	Not applicable		0.4942	0.59979	0.46338
P_{loss} (MW)			3.2669	2.9596	3.1828
L -index			0.11517	0.11298	0.13688
Emission (ton/h)			0.095747	0.093889	0.092843
Computation time (s)			1070.1630	302.5195	404.1681

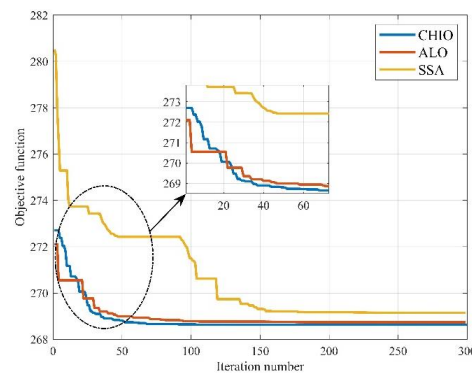


Figure 12. Convergence rates for Scenario 12 with ALO, SSA, and CHIO.

Table 18. Lists of control variables for Scenario 13 for IEEE 30-bus test scheme: TOPSIS-based solutions (The numbers in bold are the best values found).

Variables and Parameters	Min	Max	CHIO	ALO	SSA	
Active power (MW)	P_{TG2}	20	80	73.507	47.479	47.016
	P_{TG5}	10	60	54.844	45.5	47.761
	P_{TG8}	10	35	33.146	25.043	33.585
	P_{TG11}	10	60	56.072	46.144	46.941
	P_{TG13}	10	48.652	38.813	35.025	40.565
Reactive power (MVar)	Q_2	-20	60	-20	1.6023	33.452
	Q_5	-30	35	35	31.742	6.0559
	Q_8	-15	40	40	40	40
	Q_{11}	-25	30	37.94	20.115	24.597
	Q_{13}	-20	25	44.923	25	25
Bus voltage (pu)	V_1	0.96	1.10	1.0326	1.0659	1.0516
	V_2	0.96	1.10	0.97156	1.0572	1.0502
	V_5	0.96	1.10	1.0951	1.0475	1.0134
	V_8	0.96	1.10	1.0909	1.0718	1.0592
	V_{11}	0.96	1.10	1.0948	1.0763	1.0775
	V_{13}	0.96	1.10	1.0941	1.0916	1.0695
W_{gencost}			173.76	138.58	146.75	
PV_{gencost}			164.98	128.43	131.24	
$PVTP_{\text{gencost}}$			119.51	106.59	125.99	
$Fuel_{\text{vlvcost}}$			406	414.66	400.5	
Total cost (\$/h)			864.25	788.26	804.47	
VD (pu)	Not applicable		0.39559	0.55259	0.42219	
P_{loss} (MW)			3.1204	3.9664	3.4982	
L -index			0.075979	0.11077	0.10948	
Emission (ton/h)			0.096721	0.10653	0.096649	
Computation time (s)			991.7640	347.8191	358.4133	

5.1.5. Quanta-Objective Scenario

Table 18 demonstrates the results of the EETD issue for quanta-objectives “Scenario 13”. The table confirms that the presented CHIO indicates more competitive compromise alternatives at appropriate thresholds of voltage at the losses to the system in comparison with the ALO and the SSA. It can be noted from Figure 13 that the presented CHIO attains the best alternative. Furthermore, Table 19 assesses the CHIO offered as compared to MOMICA [34], I-NSGA-III [35], MODA [37], and ECHT [36] in the context of Scenario 13.

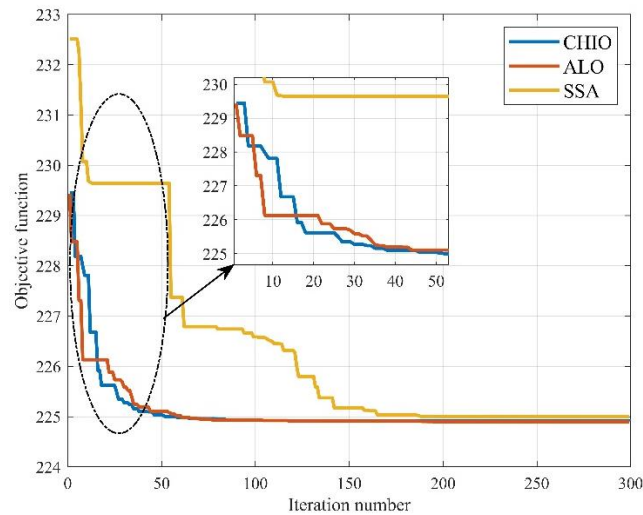


Figure 13. Convergence rates for Scenario 13 with ALO, SSA, and CHIO.

Table 19. Comparative analysis for quad and quanta objective functions (Scenarios 12 and 13) (The numbers in bold are the best values found).

Scenarios	Scenario #12				Scenario #13					
	Objective Functions	Fuel Costs (\$/h)	Emission (ton/h)	VD (pu)	Power Losses (MW)	Fuel Costs (\$/h)	Emissions (ton/h)	VD (pu)	Power Losses (MW)	L-Index
MOMICA [34]	830.188	0.252	0.298	5.585	-	-	-	-	-	-
I-NSGA-III [35]	881.9395	0.2209	0.1754	4.7449	843.8571	0.1485	0.2388	5.7405	0.1253	
MODA [37]	828.49	0.265	0.585	5.912	-	-	-	-	-	-
ECHT [36]	830.2123	0.253	0.296	5.586	-	-	-	-	-	-
PSO-SSO [72]	826.94	0.258	0.466	5.515	826.8	0.256	0.463	5.464	0.145	
ALO	769.07	0.14957	0.84792	5.5493	769.93	0.14867	0.97541	5.3714	0.11758	
SSA	770.43	0.14799	0.83337	5.4257	770.18	0.15455	0.8247	5.6446	0.12473	
CHIO	768.92	0.15177	0.92664	5.4395	770.13	0.14624	0.86862	5.3023	0.12242	

5.2. Results for IEEE 57-Bus Scheme

For SO and MO scenarios for the second test scheme, the simulation findings are stated as follows:

5.2.1. Single Objective Scenarios

For the IEEE-57 bus scheme, Table 20 shows the SOEETD alternatives obtained by the ALO, the SSA, and the presented CHIO for Scenario 14. In this scenario, the minimization of fuel costs is the main OF. The presented CHIO tends to be the least economical alternative (USD 32,752/h) in comparison with other approaches the ALO (USD 32,756/h) and the SSA (USD 32,770/h). Figure 14 illustrates the convergence rates of the proposed CHIO in comparison to other algorithms of the ALO and the SSA. This figure shows that the CHIO attains the best estimates of the OF in the least number of iterations

Table 20. Lists of control variables for Scenario 14 for IEEE 57-bus test scheme (The numbers in bold are the best values found).

Variables and Parameters		Bounds		Scenario #14		
		Min	Max	CHIO	ALO	SSA
Active power (MW)	P_{TPG1}	80	200	142.03	143.32	142.02
	P_{TPG2}	30	100	100	100	100
	P_{TPG3}	40	140	140	140	140
	P_{TPG6}	30	100	90.462	99.915	85.404
	P_{TPG8}	100	550	381.24	375.31	384.08
	P_{TPG9}	30	100	48.64	48.587	48.605
	P_{TPG12}	100	410	362.39	362.87	364.11
Reactive power (MVar)	Q_2	-17	50	46.138	49.685	50
	Q_3	-10	60	29.639	28.616	-10
	Q_6	-8	25	5.0015	1.2401	-8
	Q_8	-140	200	42.065	40.539	69.403
	Q_9	-3	9	5	9	-3
	Q_{12}	-150	155	56.541	67.292	69.611
Bus voltage (pu)	V_1	0.95	1.10	1.1	1.0991	1.1
	V_2	0.95	1.10	1.1	1.1	1.0999
	V_3	0.95	1.10	1.1	1.1	1.0078
	V_6	0.95	1.10	1.1	1.0994	0.9591
	V_8	0.95	1.10	1.1	1.1	1.1
	V_{11}	0.95	1.10	1.1	1.098	1.0423
	V_{12}	0.95	1.10	1.0821	1.0865	1.0823
$W_{\text{gen cost}}$				555.43	555.43	555.43
$PV_{\text{gen cost}}$				1646.6	1616.9	1658.4
$PVTP_{\text{gen cost}}$				156.77	156.57	156.63
$Fuel_{\text{vlv cost}}$				30,393	30,427	30,399
Fuel costs (\$/h)				Not applicable	32,752	32,770
VD (pu)				4.9146	4.9821	4.5556
P_{loss} (MW)				12.738	12.708	13.098
L -index				0.2321	0.2294	0.2417
Emissions (ton/h)				1.2322	1.2582	1.2763
Computation time (s)				347.42	399.24	609.65

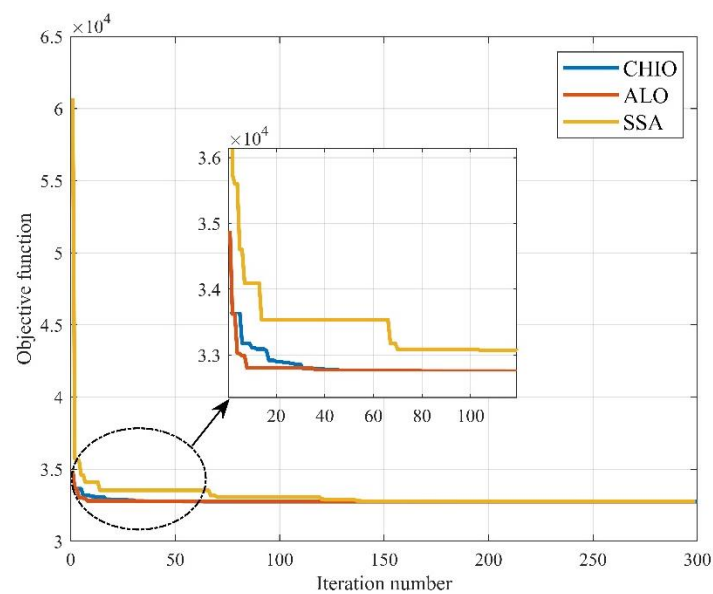


Figure 14. Convergence rates for Scenario 14 with ALO, SSA, and CHIO.

5.2.2. Dual-Objective Scenarios “Economical and Technical Benefits”

In Scenario 15, the fuel costs and *VD* can be enhanced concurrently. The presented CHIO tends to the optimal compromise alternative using the AHP (USD 32,754/h) and (4.8974 pu) in comparison with other individual approaches; the ALO (USD 32,771/h) and (4.9926 pu); and the SSA (USD 32,786/h) and (4.6149 pu). The proposed CHIO leads to the optimal compromise solution using the TOPSIS (USD 33,299/h) and (1.0707 pu) in comparison with other individual techniques; the ALO (USD 32,935/h) and (1.0937 pu); and the SSA (USD 33,230/h) and (1.0872 pu); as illustrated in Table 21. The fuel cost using the CHIO-AHP and voltage deviation using the SSA-AHP are more economical and technical than obtained using other approaches, respectively.

Table 21. Lists of control variables for Scenario 15 using AHP and TOPSIS for IEEE 57-bus test scheme (The numbers in bold are the best values found).

Variables and Parameters		Bounds		Scenario #15—AHP			Scenario #15—TOPSIS		
		Min	Max	CHIO	ALO	SSA	CHIO	ALO	SSA
Active power (MW)	<i>P_{TPG1}</i>	80	200	141.13	146.85	142.12			
	<i>P_{TPG2}</i>	30	100	100	100	100	97.284	99.802	99.991
	<i>P_{TPG3}</i>	40	140	140	140	140	136.61	139.98	140
	<i>P_{TPG6}</i>	30	100	90.525	66.72	64.232	66.124	75.725	49.604
	<i>P_{TPG8}</i>	100	550	381.28	391.52	390.9	394.54	400.59	342.82
	<i>P_{TPG9}</i>	30	100	48.555	48.524	48.595	47.437	48.526	48.244
	<i>P_{TPG12}</i>	100	410	362.39	374	375.88	349.16	360.12	406.63
Reactive power (MVar)	<i>Q₂</i>	−17	50	50	47.376	50	50	50	−17
	<i>Q₃</i>	−10	60	30.456	28.034	−10	32.267	−10	35.239
	<i>Q₆</i>	−8	25	5.0223	9.0762	−8	−8	25	25
	<i>Q₈</i>	−140	200	42.625	37.959	63.327	45.618	13.908	28.807
	<i>Q₉</i>	−3	9	9	9	9	9	9	9
	<i>Q₁₂</i>	−150	155	56.269	63.386	65.015	139.05	155	155
Bus voltage (pu)	<i>V₁</i>	0.95	1.10	1.099	1.0996	1.1	1.0096	1.0153	0.99824
	<i>V₂</i>	0.95	1.10	1.1	1.1	1.0977	1.0274	1.038	0.95031
	<i>V₃</i>	0.95	1.10	1.1	1.1	0.9876	1.0113	0.99729	1.003
	<i>V₆</i>	0.95	1.10	1.1	1.0991	1.0437	0.99375	1.0266	1.0878
	<i>V₈</i>	0.95	1.10	1.1	1.1	1.1	1.0164	1.0094	1.0091
	<i>V₁₁</i>	0.95	1.10	1.1	1.1	1.099	1.0247	1.0577	1.0997
	<i>V₁₂</i>	0.95	1.10	1.0815	1.0866	1.0836	1.0257	1.0426	1.0941
	<i>W_{gencost}</i>			555.43	555.43	555.43	539.82	555.32	555.43
	<i>PV_{gencost}</i>			1645.4	1691.9	1689.8	1706.3	1732.7	1468.1
	<i>PVTP_{gencost}</i>			156.45	156.33	156.6	152.24	156.33	155.27
	<i>Fuel_{v_{lvcost}}</i>			30,397	30,367	30,384	30,900	30,490	31,052
	Fuel costs (\$/h)			32,754	32,771	32,786	33,299	32,935	33,230
	<i>VD</i> (pu)	Not applicable		4.8974	4.9926	4.6149	1.0707	1.0937	1.0872
	<i>P_{loss}</i> (MW)			12.736	12.458	12.717	16.833	16.794	16.379
	<i>L-index</i>			0.23147	0.22979	0.2404	0.26182	0.26843	0.25241
	Emissions (ton/h)			1.2584	1.341	1.3454	1.3261	1.3465	1.3064
	Computation time (s)			427.4885	414.6923	596.62	1303.38	455.579	560.509

The fuel cost using the ALO-TOPSIS and voltage deviation using the CHIO-TOPSIS are more economical and technical than obtained using other approaches, respectively. Figure 15 shows the convergence rate and the Pareto front for the dual objectives for Scenario 15 using the AHP and the TOPSIS, respectively.

5.2.3. Dual-Objective Scenarios “Economical and Environmental Benefits”

In Scenario 16, the fuel costs and emissions are concurrently enhanced. The presented CHIO tends to be the optimal compromise alternative using the AHP (USD 32,751/h) and (1.2553 ton/h) in comparison with other approaches; the ALO (USD 32,753/h) and

(1.2581 ton/h); and the SSA (USD 32,772/h) and (1.3422 ton/h). The proposed CHIO leads to the optimal compromise alternative using the TOPSIS (USD 33,344/h) and (1.0976 ton/h) compared with other approaches; the ALO (USD 33,049/h) and (1.1198 ton/h); and the SSA (USD 33,473 /h) and (1.0964 ton/h) as illustrated in Table 22. The fuel cost and emission levels obtained using the CHIO-AHP are more economical and environmental than obtained using other approaches, respectively.

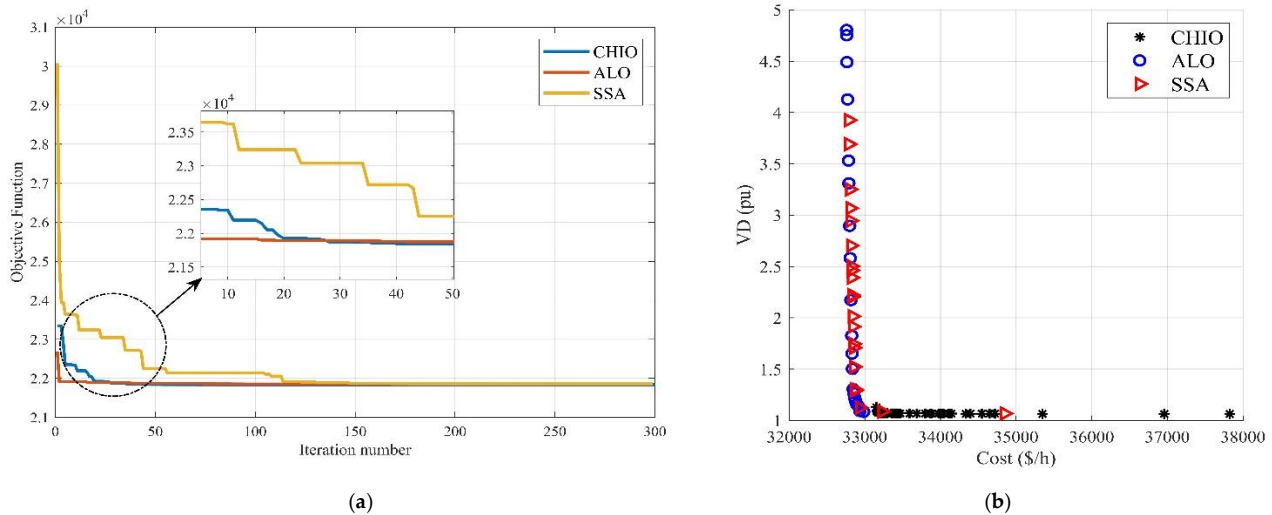


Figure 15. The convergence rate and the Pareto front for the dual-objective for Scenario 15 using the AHP and TOPSIS: (a) convergence rates using the AHP with ALO, SSA, and CHIO; (b) Pareto fronts with CHIO, ALO, and SSA.

Table 22. Lists of control variables for Scenario 16 using AHP and TOPSIS for IEEE 57-bus test scheme (The numbers in bold are the best values found).

Variables and Parameters		Bounds		Scenario #16—AHP			Scenario #16—TOPSIS		
		Min	Max	CHIO	ALO	SSA	CHIO	ALO	SSA
Active power (MW)	<i>P_{TPG1}</i>	80	200	140.44	142.84	158.66	140.44	142.84	158.66
	<i>P_{TPG2}</i>	30	100	100	100	100	100	100	99.849
	<i>P_{TPG3}</i>	40	140	140	140	140	139.99	140	139.99
	<i>P_{TPG6}</i>	30	100	90.488	95.416	65.626	99.938	100	99.78
	<i>P_{TPG8}</i>	100	550	381.21	384.31	392.53	320.04	336.72	320.58
	<i>P_{TPG9}</i>	30	100	48.653	48.614	48.601	48.609	48.671	48.578
	<i>P_{TPG12}</i>	100	410	362.38	357.39	372.12	339.96	345.59	334.15
Reactive power (MVar)	<i>Q₂</i>	−17	50	46.138	49.066	49.93	45.377	45.545	30.186
	<i>Q₃</i>	−10	60	29.64	28.429	30.756	26.853	21.835	−4.2581
	<i>Q₆</i>	−8	25	4.9955	3.4006	10.004	7.0424	4.1125	−8
	<i>Q₈</i>	−140	200	42.068	39.15	47.067	44.505	35.441	83.674
	<i>Q₉</i>	−3	9	9	9	−3	9	9	9
	<i>Q₁₂</i>	−150	155	56.541	67.055	61.353	80.818	102.34	48.528
Bus voltage (pu)	<i>V₁</i>	0.95	1.10	1.1	1.0993	1.099	1.0995	1.1	1.0934
	<i>V₂</i>	0.95	1.10	1.1	1.1	1.1	1.0994	1.1	1.0852
	<i>V₃</i>	0.95	1.10	1.1	1.1	1.1	1.0992	1.1	1.0724
	<i>V₆</i>	0.95	1.10	1.1	1.1	1.0992	1.0995	1.1	1.0496
	<i>V₈</i>	0.95	1.10	1.1	1.1	1.1	1.0987	1.1	1.0915
	<i>V₁₁</i>	0.95	1.10	1.1	1.0999	0.9527	1.0968	1.1	1.0907
	<i>V₁₂</i>	0.95	1.10	1.0821	1.0858	1.0833	1.0887	1.1	1.0614

Table 22. Cont.

Variables and Parameters	Bounds		Scenario #16—AHP			Scenario #16—TOPSIS		
	Min	Max	CHIO	ALO	SSA	CHIO	ALO	SSA
$W_{\text{gen cost}}$			555.43	555.43	555.43	555.39	555.43	555.36
$PV_{\text{gen cost}}$			1645.4	1658.3	1696.8	1363.1	1439.8	1365.3
$PVTP_{\text{gen cost}}$			156.82	156.67	156.62	156.65	156.9	156.54
$Fuel_{\text{vlvcost}}$			30,393	30,383	30,363	31,269	30,897	31,395
Fuel costs (\$/h)	Not applicable		32,751	32,753	32,772	33,344	33,049	33,473
VD (pu)			4.9146	4.9718	4.8841	4.9968	5.2342	3.8727
P_{loss} (MW)			12.738	12.968	12.601	14.258	13.762	15.241
L -index			0.2321	0.2298	0.2317	0.22947	0.22395	0.25315
Emissions (ton/h)			1.2553	1.2581	1.3422	1.0976	1.1198	1.0964
Computation time (s)			422.21	404.68	488.94	1575.13	402.319	477.557

The fuel cost using the ALO-TOPSIS and emission levels using the CHIO-TOPSIS are more economical and technical than obtained using other approaches, respectively. Figure 16 shows the convergence rate and the Pareto front for the dual objectives for Scenario 16 using the AHP and the TOPSIS, respectively.

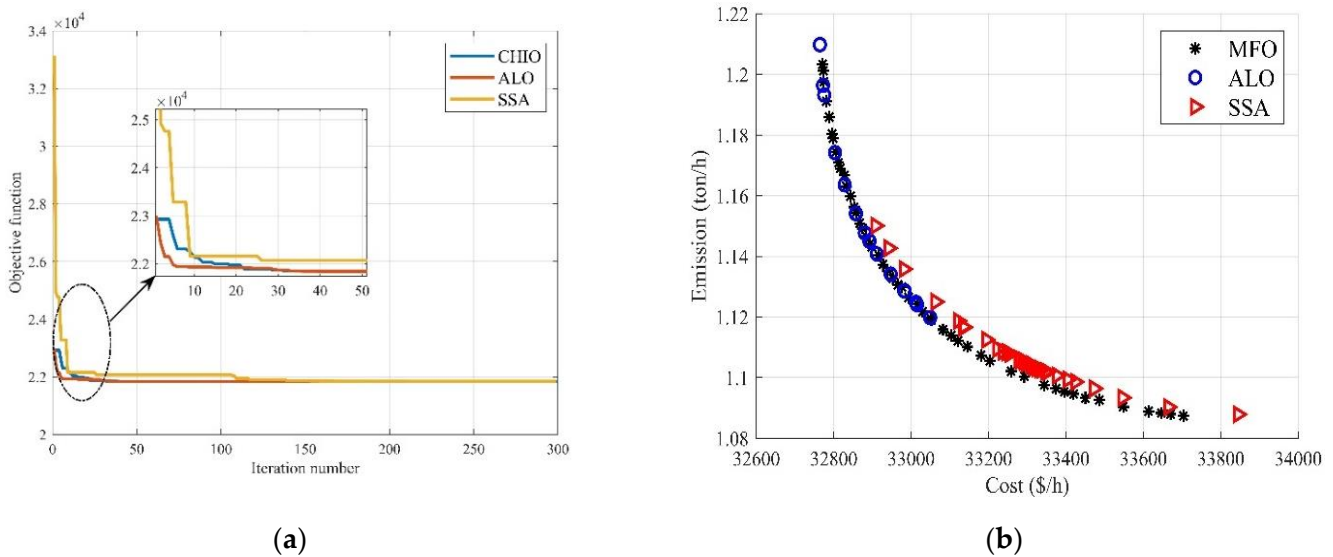


Figure 16. The convergence rate and the Pareto front for the dual objectives for Scenario 16 using AHP and TOPSIS: (a) convergence rates using AHP with ALO, SSA, and CHIO; (b) Pareto fronts with ALO, SSA, and CHIO.

5.3. Evaluation of Economical-Environmental-Technical Benefits

In this section, we focus on the economic, environmental, and technical advantages that allow the operator to compromise the various operational elements. Table 23 highlights the economic benefits of saving in fuel costs for the two standard test schemes with and without the integration of RESs using the proposed CHIO technique. This table compares the presented approach to the best approach published in the literature, which corresponds to various objectives. For the IEEE 30-bus, the annual saving differences in fuel cost with and without RESs in Scenarios 1 and 6 are USD 263,062.8 and USD 569,522.6, respectively. For the IEEE 57-bus, the annual saving differences in fuel cost with and without RESs in Scenarios 14 and 16 are USD 78,092,421.6 and USD 78,152,865.6, respectively.

Table 23. Economic benefits of the presented CHIO approach in comparison with other approaches with and without the integration of RESs.

System	Scenario #	IEEE without RESs			IEEE Integrated with RESs			Saving Difference with and without RESs			
		Competitive Techniques		Savings (\$/h)	Annual Savings (\$/yr.)	Competitive Techniques		Savings (\$/h)	Annual Savings (\$/yr.)	Savings (\$/h)	Annual Savings (\$/yr.)
IEEE 30-bus	1	PSO-SSO [72]	798.98	0.0550	481.80	CHIO	768.95	12.45	109,062	30.03	263,062.8
		ECBO [73]	799.035			GWO [76]	781.40				
	6	PSO-SSO [72]	834.804	0.110	963.60	CHIO	769.79	12.51	109,588	65.014	569,522.6
		MVO [75]	834.95			SHADE [76]	782.30				
IEEE 57-bus	14	PSO-SSO [72]	41,666.66	7.96	69,729.6	CHIO	32,752	4	35,040	8914.66	78,092,421.6
		DA-PSO [37]	41,674.62			ALO	32,756				
	16	PSO-SSO [72]	41,672.56	151.9	1,330,644	CHIO	32,751	2	17,520	8921.56	78,152,865.6
		SSO [72]	41,824.46			ALO	32,753				

Table 24 highlights the environmental benefits of saving in emission levels for the two standard test schemes with and without the integration of RESs utilizing the presented CHIO technique. For the IEEE 30-bus, the annual saving differences in emission levels with and without RESs in Scenarios 10 and 13 are 657 ton/h and 963.6 ton/h, respectively. For the IEEE 57-bus, the annual saving differences in fuel cost with and without RESs in Scenarios 14 and 16 are 973.236 ton/h and 917.172 ton/h, respectively.

Table 24. Environmental benefits of the presented CHIO approach in comparison with other approaches with and without the integration of RESs.

System	Scenario #	IEEE without RESs			IEEE Integrated with RESs			Saving Difference with and without RESs			
		Competitive Techniques		Savings (ton/h)	Annual Savings (ton/yr.)	Competitive Techniques		Savings (ton/h)	Annual Savings (ton/yr.)	Savings (ton/h)	Annual Savings (ton/yr.)
IEEE 30-bus	10	PSO-SSO [72]	0.224	0.001	8760	CHIO	0.14855	1.6115	14,116.3	0.075	657
		PSO [72]	0.225			GWO [76]	1.76				
	13	PSO-SSO [72]	0.256	0.001	8760	CHIO	0.14624	0.314	2750.6	0.11	963.6
		SSA [72]	0.257			SHADE [76]	0.46				
IEEE 57-bus	14	PSO-SSO [72]	1.3433	0.5654	4947.25	CHIO	1.2322	0.026	227.76	0.11	973.236
		DA-PSO [37]	1.9087			ALO	1.2582				
	16	PSO-SSO [72]	1.36	0.24	ALO	1.2581	1.2553	0.0028	24.528	0.105	917.172
		SSO [72]	1.60								

From the technical point of view, as seen in Table 25, the CHIO presented has the lowest level in emissions with considerable emission reductions for Scenarios 10, 13, 14, and 16 corresponding to 8760 kg, 4947 tons, and 2100 tons/yr., respectively. Table 24 highlights the technical benefits of saving in power losses for the two standard test systems with and without the integration of RESs using the presented CHIO technique. For the IEEE 30-bus, the annual saving differences in P_{loss} with and without RESs in Scenarios 1 and 4 are 26,823.12 MW and 6937.044 MW, respectively. For the IEEE 57-bus, the annual saving differences in power losses with and without RESs in Scenarios 14 and 16 are 19,096.8 MW and 21,295.56 MW, respectively.

Table 25. Technical benefits of the presented CHIO method in comparison with other methods with and without the integration of RESs.

System	Scenario #	IEEE without RESs			IEEE Integrated with RESs		Saving Difference with and without RESs	
		Competitive Techniques	Savings (MW)	Annual Savings (MW)	Competitive Techniques	Savings (MW)	Annual Savings (MW/yr.)	
IEEE 30-bus	1	PSO-SSO [72]	8.602	98.112	CHIO	5.54	3.062	26,823.12
		ECBO [73]	8.6132					
	4	PSO-SSO [72]	2.858	201.48	CHIO	2.0661	0.7919	6937.044
		MVO [75]	2.881					
IEEE 57-bus	14	PSO-SSO [72]	14.916	192.72	CHIO	12.736	2.18	19,096.8
		DA-PSO [37]	14.938					
	16	PSO-SSO [72]	15.169	1900.9	CHIO	12.738	2.431	21,295.56
		SSO [72]	15.386					

6. Conclusions

This paper proposed an EETD problem for obtaining the best compromise solutions; fuel costs, emission levels, voltage deviation, losses, and stability index of adapted IEEE 30-bus and IEEE 57-bus schemes involved thermal and RESs such as PV, wind, and hybrid PV and tidal-power plants. The major objective is to keep overall fuel costs, active power losses, and pollution levels as low as possible. Various constraints were studied as system limitations. Different optimization methods—the CHIO, the SSA, and the ALO—were utilized for identifying the best alternatives. A total of 16 scenarios were assessed to confirm the potential of the introduced model in resolving the EETD issue. The AHP was employed in computing the weights of the EETD issue. In addition, the TOPSIS procedure was developed to help decision makers use various preferences to find the best alternatives from Pareto results. Finally, the results showed that the CHIO surpasses the techniques studied in resolving the EETD problem. By applying additional optimization techniques, especially hybrid algorithms, the EETD formula may be further researched. Furthermore, it is still a challenge for future study that non-convex EETD problems and uncertainties about load demand combined with uncertainties of all RESs be explored. In addition, IEEE 118 bus, including thermal and stochastic RESs, can be investigated in future works.

Author Contributions: B.S.M. and Z.M.A. designed the case under study, performed the simulations and obtained the results; A.I.O. and S.H.E.A.A. analyzed the obtained results; B.S.M. and A.I.O. wrote the paper, which S.H.E.A.A. and Z.M.A. reviewed further. All authors have read and agreed to the published version of the manuscript.

Funding: The authors extend their appreciation to the Deputy ship for the Research & innovation, Ministry of Education in Saudi Arabia for funding this research work through the project number (IF-PSAU-2021/01/17642).

Data Availability Statement: The data presented in this study are available on request from the corresponding author. The data are not publicly available due to their large size.

Conflicts of Interest: The authors declare no conflict of interest.

Abbreviations

ABC	Artificial bee colony
ABC-DP	Dynamic population-based artificial bee colony
AHP	Analytical hierarchy process
ALO	Ant lion optimizer
APSO	Accelerating particle swarm optimization
CCO	Criss-cross optimizer

CHIO	Coronavirus herd immunity optimizer
CI	Consistency index
CR	Consistency ratio
DP	Dynamic programming
EETD	Economical-environmental-technical dispatch
ES	Energy storage
ESCO	Enhanced sine cosine optimizer
GF	Gumbel fitting
HIP	Herd immunity population
HIS	Herd immunity size
ISA	Interior search algorithm
LF	Lognormal fitting
MADM	Multi-attribute decision making
MIL	Mixed-integer linear
MIQ	Mixed-integer quadratic
MO	Multi-objective
MOCE/D	Multi-objective cross-entropy algorithm based on decomposition
MOEA/D	Decomposition-based multi-objective evolutionary algorithm
MOHHO	Multi-objective Harris hawks optimization
MOPEO	Multi-objective population extremal optimization
MWOA	Modified whale optimization algorithm
NSGA	Non-dominated sorting genetic algorithm
NSGA-RL	Non-dominated sorting genetic algorithm reinforcement learning
ORC	Overestimation of the reservation cost
PDFs	Probability density functions
POZs	Prohibited operating zones
PSO	Particle swarm optimization
PV	photovoltaic
PVTP	Photovoltaic and tidal power
RC	Relative closeness
RESs	Renewable energy sources
RI	Average random index
SMODE	Summation based multi-objective differential evolution
SO	Single objective
SOS	Symbiotic organisms search
SPG	Standby power generation
SSA	Salp swarm algorithm
TLBO	Teaching learning-based optimization
TOPSIS	The technique for order preference by similarity to an ideal solution
TP	Tidal power
TPGs	Thermal power generations
TVAC	Time-varying acceleration coefficient
UPC	Underestimation of the penalty cost
VD	Voltage deviation
WF	Weibull fitting
WP	Wind power

Nomenclature

α	The scale factor of the wind turbine
β	The shape factor of the wind turbine
$C_{d_{PV}}$	The direct cost of the photovoltaic system
$C_{d_{PVTP}}$	The direct cost of the photovoltaic-tidal power system
$C_{d_{WP}}$	The direct cost of the wind turbine
$C_{r_{PV}}$	The reserve capacity cost of the photovoltaic system
$C_{r_{PVTP}}$	The reserve capacity cost of the photovoltaic-small hydro system
$C_{r_{WP}}$	The reserve capacity cost of the wind turbine
$C_{S_{PV}}$	The storage units cost of the photovoltaic system
$C_{S_{PVTP}}$	The storage units cost of the photovoltaic-tidal power system

C_{SWP}	The storage units cost of the wind turbine
C_{tot}	The total cost of the fuel or generation
C_{totPV}	The total cost of the photovoltaic generation unit
$C_{totPVTP}$	The total cost of the photovoltaic-tidal power unit
C_{totWP}	The total cost of the wind turbine generation unit
$C_{tot}(P_{TPGs})$	The total cost of the thermal power generations
$C_{tot}(P_{RESs})$	The total cost of the renewable energy sources
δ_{ij}	The phase difference between the buses i and j
η_w	Tidal efficiency turbines'
E_{tot}	The total emission
$f_v(v)$	The probability of wind speed
f	Friction factor
γ	Scale parameter of the river
G	Solar irradiance
G_{std}	Standard solar irradiance
$G_{q(ij)}$	The transconductance of branch q connected to bus i and bus j
H_w	The effective pressure head for the water
K_{dWP}	The direct cost parameter of the wind turbine
K_{rWP}	The reserve capacity cost parameter of the wind turbine
K_{SWP}	The storage unit cost parameter of the wind turbine
λ	Location parameter of the river
L -index	Stability index
Max_Itr	Maximum iteration number
N_G	Number of generator buses
N_L	Number of load buses
nl	Number of branches in the network
P_{loss}	Power loss
P_{PVact}	The actual power of the photovoltaic system
P_{PVr}	The rated power of the photovoltaic system
P_{PVsch}	The scheduled power of the photovoltaic system
$P_{PVTPact}$	The actual power of the photovoltaic small hydro system
$P_{PVTPsch}$	The scheduled power of the photovoltaic-small hydro system
$P_{TPG_i}^{min}$	The minimum power of the i th thermal power generator unit
$P_T(Q_w)$	The yield power from the tidal power plant
P_{WPact}	The actual power of the wind turbine
P_{WP_r}	The rated power of the wind turbine
P_{WPsch}	The scheduled power of the wind turbine
Q_w	River flow rate
R_c	Operation irradiance
ρ_w	Water density
S_{Lp}	The branches' capacity limit
T_s	The standard temperature in kelvin
v	The wind speed
V_{G_i}	The voltage of the i th on generator bus
v_{in}	Cut-in speed of the wind turbine
V_{Lp}	The voltage of the p th on load bus
v_{out}	Cut-out speed of the wind turbine
v_r	The rated speed of the wind turbine

Appendix A

Table A1. Direct, reserve, and standby cost coefficients for RESs uncertainties.

	WP	PV	PVTP
Direct cost coefficients (\$/MW)	$K_{dWP} = 1.70$	$K_{dPV} = 1.60$	$K_{dPVTP} = 1.50$
Reserve cost coefficients (\$/MW)	$K_{rWP} = 3.00$	$K_{rPV} = 3.00$	$K_{rPVTP} = 3.00$
Penalty cost coefficients (\$/MW)	$K_{SWP} = 1.40$	$K_{SPV} = 1.40$	$K_{SPVTP} = 1.40$

Table A2. Control parameter setting of CHIO, ALO, and SSA algorithms for the testing power system.

Optimization Techniques	ALO	SSA	Proposed (CHIO)
Max. iteration	300	300	300
No. of population	50	50	50
Control parameters	rand = [0, 1]	$K_{min} = 0.43$ $K_{max} = 0.85$	$C_0 = 1$ $BR_r = 0.05$
Independent runs	30	30	30

Table A3. Decision variables of the IEEE 30-bus system.

Decision Variables		Bounds	
		Min	Max
Active power (MW)	P_{TPG2}	20	80
	P_{TPG5}	10	60
	P_{TPG8}	10	35
	P_{TPG11}	10	60
	P_{TPG13}	10	60
Bus voltage (pu)	V_1	0.96	1.10
	V_2	0.96	1.10
	V_5	0.96	1.10
	V_8	0.96	1.10
	V_{11}	0.96	1.10
	V_{13}	0.96	1.10

Table A4. Decision variables of the IEEE 57-bus system.

Decision Variables		Bounds	
		Min	Max
Active power (MW)	P_{TPG1}	80	200
	P_{TPG2}	30	100
	P_{TPG3}	40	140
	P_{TPG6}	30	100
	P_{TPG8}	100	550
	P_{TPG9}	30	100
	P_{TPG12}	100	410
Bus voltage (pu)	V_1	0.95	1.10
	V_2	0.95	1.10
	V_3	0.95	1.10
	V_6	0.95	1.10
	V_8	0.95	1.10
	V_{11}	0.95	1.10
	V_{12}	0.95	1.10

References

- Omar, A.I.; Khattab, N.M.; Abdel Aleem, S.H.E. Optimal strategy for transition into net-zero energy in educational buildings: A case study in El-Shorouk City, Egypt. *Sustain. Energy Technol. Assess.* **2022**, *49*, 101701. [\[CrossRef\]](#)
- Ahmed, E.M.; Rathinam, R.; Dayalan, S.; Fernandez, G.S.; Ali, Z.M.; Abdel Aleem, S.H.E.; Omar, A.I. A Comprehensive Analysis of Demand Response Pricing Strategies in a Smart Grid Environment Using Particle Swarm Optimization and the Strawberry Optimization Algorithm. *Mathematics* **2021**, *9*, 2338. [\[CrossRef\]](#)
- Elmetwaly, A.H.; ElDesouky, A.A.; Omar, A.I.; Attya Saad, M. Operation control, energy management, and power quality enhancement for a cluster of isolated microgrids. *Ain Shams Eng. J.* **2022**, *13*, 101737. [\[CrossRef\]](#)
- McLarty, D.; Panossian, N.; Jabbari, F.; Traverso, A. Dynamic economic dispatch using complementary quadratic programming. *Energy* **2019**, *166*, 755–764. [\[CrossRef\]](#)
- Zhan, J.P.; Wu, Q.H.; Guo, C.X.; Zhou, X.X. Fast λ -Iteration Method for Economic Dispatch With Prohibited Operating Zones. *IEEE Trans. Power Syst.* **2014**, *29*, 990–991. [\[CrossRef\]](#)
- Elsheakh, Y.; Zou, S.; Ma, Z.; Zhang, B. Decentralised gradient projection method for economic dispatch problem with valve point effect. *IET Gener. Transm. Distrib.* **2018**, *12*, 3844–3851. [\[CrossRef\]](#)

7. Mahdi, F.P.; Vasant, P.; Kallimani, V.; Watada, J.; Fai, P.Y.S.; Abdullah-Al-Wadud, M. A holistic review on optimization strategies for combined economic emission dispatch problem. *Renew. Sustain. Energy Rev.* **2018**, *81*, 3006–3020. [[CrossRef](#)]
8. Pan, S.; Jian, J.; Yang, L. A hybrid MILP and IPM approach for dynamic economic dispatch with valve-point effects. *Int. J. Electr. Power Energy Syst.* **2018**, *97*, 290–298. [[CrossRef](#)]
9. Chen, F.; Huang, G.H.; Fan, Y.R.; Liao, R.F. A nonlinear fractional programming approach for environmental–economic power dispatch. *Int. J. Electr. Power Energy Syst.* **2016**, *78*, 463–469. [[CrossRef](#)]
10. Wang, M.Q.; Gooi, H.B.; Chen, S.X.; Lu, S. A Mixed Integer Quadratic Programming for Dynamic Economic Dispatch With Valve Point Effect. *IEEE Trans. Power Syst.* **2014**, *29*, 2097–2106. [[CrossRef](#)]
11. Pan, S.; Jian, J.; Chen, H.; Yang, L. A full mixed-integer linear programming formulation for economic dispatch with valve-point effects, transmission loss and prohibited operating zones. *Electr. Power Syst. Res.* **2020**, *180*, 106061. [[CrossRef](#)]
12. Naderi, E.; Pourakbari-Kasmaei, M.; Cerna, F.V.; Lehtonen, M. A novel hybrid self-adaptive heuristic algorithm to handle single-and multi-objective optimal power flow problems. *Int. J. Electr. Power Energy Syst.* **2021**, *125*, 106492. [[CrossRef](#)]
13. Omar, A.I.; Ali, Z.M.; Al-Gabalawy, M.; Abdel Aleem, S.H.E.; Al-Dhaifallah, M. Multi-objective environmental economic dispatch of an electricity system considering integrated natural gas units and variable renewable energy sources. *Mathematics* **2020**, *8*, 1100. [[CrossRef](#)]
14. Nourianfar, H.; Abdi, H. Solving the multi-objective economic emission dispatch problems using Fast Non-Dominated Sorting TVAC-PSO combined with EMA. *Appl. Soft Comput.* **2019**, *85*, 105770. [[CrossRef](#)]
15. Elsakaan, A.A.; El-Sehiemy, R.A.; Kaddah, S.S.; Elsaied, M.I. An enhanced moth-flame optimizer for solving non-smooth economic dispatch problems with emissions. *Energy* **2018**, *157*, 1063–1078. [[CrossRef](#)]
16. ben oualid Medani, K.; Sayah, S.; Bekrar, A. Whale optimization algorithm based optimal reactive power dispatch: A case study of the Algerian power system. *Electr. Power Syst. Res.* **2018**, *163*, 696–705. [[CrossRef](#)]
17. Karthik, N.; Parvathy, A.K.; Arul, R. Multi-objective economic emission dispatch using interior search algorithm. *Int. Trans. Electr. Energy Syst.* **2019**, *29*, e2683. [[CrossRef](#)]
18. Chinnadurrai, C.; Victoire, T.A.A. Dynamic Economic Emission Dispatch Considering Wind Uncertainty Using Non-Dominated Sorting Crisscross Optimization. *IEEE Access* **2020**, *8*, 94678–94696. [[CrossRef](#)]
19. El Sehiemy, R.A.; Selim, F.; Bentouati, B.; Abido, M.A. A novel multi-objective hybrid particle swarm and salp optimization algorithm for technical-economical-environmental operation in power systems. *Energy* **2020**, *193*, 116817. [[CrossRef](#)]
20. Biswas, P.P.; Suganthan, P.N.; Qu, B.Y.; Amaratunga, G.A.J. Multiobjective economic-environmental power dispatch with stochastic wind-solar-small hydro power. *Energy* **2018**, *150*, 1039–1057. [[CrossRef](#)]
21. El-Fergany, A.A.; Hasanien, H.M. Salp swarm optimizer to solve optimal power flow comprising voltage stability analysis. *Neural Comput. Appl.* **2020**, *32*, 5267–5283. [[CrossRef](#)]
22. Alkoffash, M.S.; Awadallah, M.A.; Alweshah, M.; Zitar, R.A.; Assaleh, K.; Al-Betar, M.A. A Non-convex Economic Load Dispatch Using Hybrid Salp Swarm Algorithm. *Arab. J. Sci. Eng.* **2021**, *46*, 8721–8740. [[CrossRef](#)]
23. Ding, M.; Chen, H.; Lin, N.; Jing, S.; Liu, F.; Liang, X.; Liu, W. Dynamic population artificial bee colony algorithm for multi-objective optimal power flow. *Saudi J. Biol. Sci.* **2017**, *24*, 703–710. [[CrossRef](#)] [[PubMed](#)]
24. Liang, R.-H.; Wu, C.-Y.; Chen, Y.-T.; Tseng, W.-T. Multi-objective dynamic optimal power flow using improved artificial bee colony algorithm based on Pareto optimization. *Int. Trans. Electr. Energy Syst.* **2016**, *26*, 692–712. [[CrossRef](#)]
25. Chen, M.-R.; Zeng, G.-Q.; Lu, K.-D. Constrained multi-objective population extremal optimization based economic-emission dispatch incorporating renewable energy resources. *Renew. Energy* **2019**, *143*, 277–294. [[CrossRef](#)]
26. Wang, G.; Zha, Y.; Wu, T.; Qiu, J.; Peng, J.; Xu, G. Cross entropy optimization based on decomposition for multi-objective economic emission dispatch considering renewable energy generation uncertainties. *Energy* **2020**, *193*, 116790. [[CrossRef](#)]
27. Duman, S.; Li, J.; Wu, L. AC optimal power flow with thermal–wind–solar–tidal systems using the symbiotic organisms search algorithm. *IET Renew. Power Gener.* **2021**, *15*, 278–296. [[CrossRef](#)]
28. Bora, T.C.; Mariani, V.C.; Coelho, L.d.S. Multi-objective optimization of the environmental-economic dispatch with reinforcement learning based on non-dominated sorting genetic algorithm. *Appl. Therm. Eng.* **2019**, *146*, 688–700. [[CrossRef](#)]
29. Yin, Y.; Liu, T.; He, C. Day-ahead stochastic coordinated scheduling for thermal-hydro-wind-photovoltaic systems. *Energy* **2019**, *187*, 115944. [[CrossRef](#)]
30. Elattar, E.E. Environmental economic dispatch with heat optimization in the presence of renewable energy based on modified shuffle frog leaping algorithm. *Energy* **2019**, *171*, 256–269. [[CrossRef](#)]
31. Attia, A.-F.; El Sehiemy, R.A.; Hasanien, H.M. Optimal power flow solution in power systems using a novel Sine-Cosine algorithm. *Int. J. Electr. Power Energy Syst.* **2018**, *99*, 331–343. [[CrossRef](#)]
32. Li, X.; Wang, W.; Wang, H.; Wu, J.; Fan, X.; Xu, Q. Dynamic environmental economic dispatch of hybrid renewable energy systems based on tradable green certificates. *Energy* **2020**, *193*, 116699. [[CrossRef](#)]
33. Chen, G.; Yi, X.; Zhang, Z.; Lei, H. Solving the Multi-Objective Optimal Power Flow Problem Using the Multi-Objective Firefly Algorithm with a Constraints-Prior Pareto-Domination Approach. *Energies* **2018**, *11*, 3438. [[CrossRef](#)]
34. Ghasemi, M.; Ghavidel, S.; Ghanbarian, M.M.; Gharibzadeh, M.; Azizi Vahed, A. Multi-objective optimal power flow considering the cost, emission, voltage deviation and power losses using multi-objective modified imperialist competitive algorithm. *Energy* **2014**, *78*, 276–289. [[CrossRef](#)]

35. Zhang, J.; Wang, S.; Tang, Q.; Zhou, Y.; Zeng, T. An improved NSGA-III integrating adaptive elimination strategy to solution of many-objective optimal power flow problems. *Energy* **2019**, *172*, 945–957. [[CrossRef](#)]
36. Biswas, P.P.; Suganthan, P.N.; Mallipeddi, R.; Amaratunga, G.A.J. Optimal power flow solutions using differential evolution algorithm integrated with effective constraint handling techniques. *Eng. Appl. Artif. Intell.* **2018**, *68*, 81–100. [[CrossRef](#)]
37. Khunkitti, S.; Siritaratiwat, A.; Premrudeepreechacharn, S.; Chatthaworn, R.; Watson, N. A Hybrid DA-PSO Optimization Algorithm for Multiobjective Optimal Power Flow Problems. *Energies* **2018**, *11*, 2270. [[CrossRef](#)]
38. Kumari, M.S.; Maheswarapu, S. Enhanced Genetic Algorithm based computation technique for multi-objective Optimal Power Flow solution. *Int. J. Electr. Power Energy Syst.* **2010**, *32*, 736–742. [[CrossRef](#)]
39. Mandal, B.; Kumar Roy, P. Multi-objective optimal power flow using quasi-oppositional teaching learning based optimization. *Appl. Soft Comput.* **2014**, *21*, 590–606. [[CrossRef](#)]
40. Roy, P.K.; Paul, C. Optimal power flow using krill herd algorithm. *Int. Trans. Electr. Energy Syst.* **2015**, *25*, 1397–1419. [[CrossRef](#)]
41. Hariharan, T.; Mohana Sundaram, K. Multiobjective optimal power flow using Particle Swarm Optimization. *Int. J. Control Theory Appl.* **2016**, *9*, 671–679.
42. Mohamed, A.-A.A.; Mohamed, Y.S.; El-Gaafary, A.A.M.; Hemeida, A.M. Optimal power flow using moth swarm algorithm. *Electr. Power Syst. Res.* **2017**, *142*, 190–206. [[CrossRef](#)]
43. Mondal, S.; Bhattacharya, A.; nee Dey, S.H. Multi-objective economic emission load dispatch solution using gravitational search algorithm and considering wind power penetration. *Int. J. Electr. Power Energy Syst.* **2013**, *44*, 282–292. [[CrossRef](#)]
44. Younes, M.; Khodja, F.; Kherfane, R.L. Multi-objective economic emission dispatch solution using hybrid FFA (firefly algorithm) and considering wind power penetration. *Energy* **2014**, *67*, 595–606. [[CrossRef](#)]
45. Qu, B.Y.; Liang, J.J.; Zhu, Y.S.; Wang, Z.Y.; Suganthan, P.N. Economic emission dispatch problems with stochastic wind power using summation based multi-objective evolutionary algorithm. *Inf. Sci.* **2016**, *351*, 48–66. [[CrossRef](#)]
46. Zhu, Y.; Wang, J.; Qu, B. Multi-objective economic emission dispatch considering wind power using evolutionary algorithm based on decomposition. *Int. J. Electr. Power Energy Syst.* **2014**, *63*, 434–445. [[CrossRef](#)]
47. Li, M.S.; Wu, Q.H.; Ji, T.Y.; Rao, H. Stochastic multi-objective optimization for economic-emission dispatch with uncertain wind power and distributed loads. *Electr. Power Syst. Res.* **2014**, *116*, 367–373. [[CrossRef](#)]
48. Bilil, H.; Aniba, G.; Maaroufi, M. Probabilistic Economic Emission Dispatch Optimization of Multi-sources Power System. *Energy Procedia* **2014**, *50*, 789–796. [[CrossRef](#)]
49. Khan, N.; Sidhu, G.; Gao, F. Optimizing Combined Emission Economic Dispatch for Solar Integrated Power Systems. *IEEE Access* **2016**, *4*, 1. [[CrossRef](#)]
50. Shilaja, C.; Ravi, K. Optimization of emission/economic dispatch using euclidean affine flower pollination algorithm (eFPA) and binary FPA (BFPA) in solar photo voltaic generation. *Renew. Energy* **2017**, *107*, 550–566. [[CrossRef](#)]
51. Roy, R.; Jadhav, H.T. Optimal power flow solution of power system incorporating stochastic wind power using Gbest guided artificial bee colony algorithm. *Int. J. Electr. Power Energy Syst.* **2015**, *64*, 562–578. [[CrossRef](#)]
52. Rawa, M.; Abusorrah, A.; Bassi, H.; Mekhilef, S.; Ali, Z.M.; Abdel Aleem, S.H.E.; Hasanien, H.M.; Omar, A.I. Economical-technical-environmental operation of power networks with wind-solar-hydropower generation using analytic hierarchy process and improved grey wolf algorithm. *Ain Shams Eng. J.* **2021**, *12*, 2717–2734. [[CrossRef](#)]
53. Mirjalili, S.; Gandomi, A.H.; Mirjalili, S.Z.; Saremi, S.; Faris, H.; Mirjalili, S.M. Salp Swarm Algorithm: A bio-inspired optimizer for engineering design problems. *Adv. Eng. Softw.* **2017**, *114*, 163–191. [[CrossRef](#)]
54. Mirjalili, S. The Ant Lion Optimizer. *Adv. Eng. Softw.* **2015**, *83*, 80–98. [[CrossRef](#)]
55. Biswas, P.P.; Suganthan, P.N.; Mallipeddi, R.; Amaratunga, G.A.J. Multi-objective optimal power flow solutions using a constraint handling technique of evolutionary algorithms. *Soft Comput.* **2020**, *24*, 2999–3023. [[CrossRef](#)]
56. Al-Gabalawy, M.; Hosny, N.S.; Dawson, J.A.; Omar, A.I. State of charge estimation of a Li-ion battery based on extended Kalman filtering and sensor bias. *Int. J. Energy Res.* **2021**, *45*, 6708–6726. [[CrossRef](#)]
57. Hulio, Z.H.; Jiang, W.; Rehman, S. Techno-Economic assessment of wind power potential of Hawke’s Bay using Weibull parameter: A review. *Energy Strateg. Rev.* **2019**, *26*, 100375. [[CrossRef](#)]
58. Qais, M.H.; Hasanien, H.M.; Alghuwainem, S. Low voltage ride-through capability enhancement of grid-connected permanent magnet synchronous generator driven directly by variable speed wind turbine: A review. *J. Eng.* **2017**, *2017*, 1750–1754. [[CrossRef](#)]
59. Hamilton, W.T.; Husted, M.A.; Newman, A.M.; Braun, R.J.; Wagner, M.J. Dispatch optimization of concentrating solar power with utility-scale photovoltaics. *Optim. Eng.* **2020**, *21*, 335–369. [[CrossRef](#)]
60. de la Calle, A.; Bayon, A.; Pye, J. Techno-economic assessment of a high-efficiency, low-cost solar-thermal power system with sodium receiver, phase-change material storage, and supercritical CO₂ recompression Brayton cycle. *Sol. Energy* **2020**, *199*, 885–900. [[CrossRef](#)]
61. Gómez, Y.M.; Bolfarine, H.; Gómez, H.W. Gumbel distribution with heavy tails and applications to environmental data. *Math. Comput. Simul.* **2019**, *157*, 115–129. [[CrossRef](#)]
62. Eshra, N.M.; Zobaa, A.F.; Abdel Aleem, S.H.E. Assessment of mini and micro hydropower potential in Egypt: Multi-criteria analysis. *Energy Rep.* **2021**, *7*, 81–94. [[CrossRef](#)]
63. Al-Betar, M.A.; Alyasseri, Z.A.A.; Awadallah, M.A.; Abu Doush, I. Coronavirus herd immunity optimizer (CHIO). *Neural Comput. Appl.* **2021**, *33*, 5011–5042. [[CrossRef](#)] [[PubMed](#)]

64. Kumar, C.; Magdalin Mary, D.; Gunasekar, T. MOCHIO: A Novel Multi-Objective Coronavirus Herd Immunity Optimization Algorithm for Solving Brushless Direct Current Wheel Motor Design Optimization Problem. *Automatika* **2021**, *63*, 149–170. [[CrossRef](#)]
65. Abdel Aleem, S.H.E.; Zobaa, A.F.; Abdel Mageed, H.M. Assessment of energy credits for the enhancement of the Egyptian Green Pyramid Rating System. *Energy Policy* **2015**, *87*, 407–416. [[CrossRef](#)]
66. Ho, W.; Ma, X. The state-of-the-art integrations and applications of the analytic hierarchy process. *Eur. J. Oper. Res.* **2018**, *267*, 399–414. [[CrossRef](#)]
67. Saaty, R.W. The analytic hierarchy process—what it is and how it is used. *Math. Model.* **1987**, *9*, 161–176. [[CrossRef](#)]
68. Beynon, M.J. Analytic Hierarchy Process. In *The SAGE Dictionary of Quantitative Management Research*; SAGE Publications Ltd.: London, UK, 2014; pp. 9–12.
69. Deb, M.; Debbarma, B.; Majumder, A.; Banerjee, R. Performance –emission optimization of a diesel-hydrogen dual fuel operation: A NSGA II coupled TOPSIS MADM approach. *Energy* **2016**, *117*, 281–290. [[CrossRef](#)]
70. Herbadji, O.; Slimani, L.; Bouktir, T. Optimal power flow with four conflicting objective functions using multiobjective ant lion algorithm: A case study of the algerian electrical network. *Iran. J. Electr. Electron. Eng.* **2019**, *15*, 94–113. [[CrossRef](#)]
71. Herbadji, O.; Slimani, L.; Bouktir, T. Multi-objective optimal power flow considering the fuel cost, emission, voltage deviation and power losses using Multi-Objective Dragonfly algorithm. In Proceedings of the International Conference on Recent Advances in Electrical Systems, Bangalore, India, 16–17 March 2017; pp. 191–197.
72. Zobaa, A.F.; Aleem, S.H.E.A.; Abdelaziz, A.Y. *Classical and Recent Aspects of Power System Optimization*; Academic Press: Cambridge, MA, USA; Elsevier: Amsterdam, The Netherlands, 2018; ISBN 9780128124413.
73. Bouchekara, H.R.E.H.; Chaib, A.E.; Abido, M.A.; El-Sehiemy, R.A. Optimal power flow using an Improved Colliding Bodies Optimization algorithm. *Appl. Soft Comput. J.* **2016**, *42*, 119–131. [[CrossRef](#)]
74. Shilaja, C.; Ravi, K. Optimal Power Flow Using Hybrid DA-APSO Algorithm in Renewable Energy Resources. *Proc. Energy Procedia* **2017**, *117*, 1085–1092. [[CrossRef](#)]
75. Roa-Sepulveda, C.A.; Pavez-Lazo, B.J. A solution to the optimal power flow using simulated annealing. In Proceedings of the 2001 IEEE Porto Power Tech Proceedings, Porto, Portugal, 10–13 September 2001; Volume 2, pp. 5–9. [[CrossRef](#)]
76. Khan, I.U.; Javaid, N.; Gamage, K.A.A.; James Taylor, C.; Baig, S.; Ma, X. Heuristic Algorithm Based Optimal Power Flow Model Incorporating Stochastic Renewable Energy Sources. *IEEE Access* **2020**, *8*, 148622–148643. [[CrossRef](#)]